



# Development of thin film nanocomposite membrane incorporated with mesoporous synthetic hectorite and MSH@UiO-66-NH<sub>2</sub> nanoparticles for efficient targeted feeds separation, and antibacterial performance

Moucham Borpatra Gohain<sup>a,1</sup>, Radheshyam R. Pawar<sup>b,1</sup>, Sachin Karki<sup>a,c</sup>, Aditi Hazarika<sup>a</sup>, Swapnali Hazarika<sup>a,c</sup>, Pravin G. Ingole<sup>a,c,\*</sup>

<sup>a</sup> Chemical Engineering Group, Engineering Sciences and Technology Division, CSIR-North East Institute of Science and Technology, Jorhat, Assam 785006, India

<sup>b</sup> Ashapura International Limited, Survey No. 256/3, Village Baraya, Bhuj-Mundra Highway, Mundra, Kutch, Gujarat 370-415, India

<sup>c</sup> Academy of Scientific and Innovative Research (AcSIR), CSIR-NEIST Campus, Jorhat, Assam 785006, India

## ARTICLE INFO

### Keywords:

Polysulfone membrane  
Metal organic frameworks  
Synthetic hectorite  
Interfacial polymerization  
Thin film nanocomposite membranes  
Membranes separation and antibacterial performance

## ABSTRACT

Functionalized metal-organic frameworks (MOFs) and their composites are found one of the best material to develop the thin-film nanocomposite (TFN) membranes and concern water purification technologies with boosted water flux and targeted feeds rejection performance. MOFs with suitable functionalities are found more stable and efficient due to strong interfacial polymerization with free functional groups which consequently resulted in a thin selective nanocomposite layer on the surface of polysulfone flat sheet membranes. Similarly, mesoporous synthetic hectorite (MSH), due to negative surface charge acts as the best support material to avoid high agglomeration of positively charged MOF crystals. Additionally, surface hydroxyl functionalities with high dispersion capability in a polymer monomer solution makes MSH as a promising material for MOF support and development of novel membranes. Herein considering all these advantageous aspects of both material, we have established a novel approach for developing of TFN membranes by incorporating MSH, and composite of MSH and MOF (UiO-66-NH<sub>2</sub>) nanoparticles in piperazine (PIP) aqueous monomer solution, which were further interfacially polymerized with trimesoyl chloride (TMC) organic phase monomer. The developed nanoparticles (MSH and MSH@UiO-66-NH<sub>2</sub>) formulation were confirmed by ideal characterization techniques such as, PXRD, FTIR, TGA and SEM. Whereas, alteration impact of MSH and MSH@UiO-66-NH<sub>2</sub> nanoparticles on prepared membranes were physicochemically evaluated with original TFC membrane by ATR-FTIR, FE-SEM, HR-TEM, AFM, XPS, TGA, zeta potential and contact angle analysing techniques. The efficacy performance of the developed TFN membranes were compared with thin-film composite (TFC) membrane and found that TFN membranes showed excellent water flux and rejection performances against different synthetic feed solutions including most common salts (i. e. NaCl, Na<sub>2</sub>SO<sub>4</sub>, CuSO<sub>4</sub>, MgSO<sub>4</sub>, MnSO<sub>4</sub>), toxic boron in the seawater and bulky humic substances. Interestingly upon incorporation of a small amount of (0.01%) MSH and MSH@UiO-66-NH<sub>2</sub> nanoparticles into the developed membrane dramatically improved rejection performance against applied feed solutions in the trend of TFC < MSH-TFN < MSH@UiO-66-NH<sub>2</sub>-TFN. The highest rejection 94.42% for MgSO<sub>4</sub> was obtained along with the flux 34.78 L/m<sup>2</sup>.h at 1.5 MPa. Likewise, 69.56 L/m<sup>2</sup>.h flux with 71.23% rejection for boron at pH 8 (close to sea water) at 1.5 MPa. Due to hydrophilic and notable antifouling nature of TFN membranes the tested membrane shows excellent humic acid permeate flux of 80.68 L/m<sup>2</sup>.h and rejection of 98.96%. Besides, MSH@UiO-66-NH<sub>2</sub>-TFN membrane showed noteworthy antibacterial properties with efficient reduction in the bacterial colony growth. We believed that the present novel membrane modification approach has high potential in the development of high efficient water purification technologies in future.

\* Corresponding author. Chemical Engineering Group, Engineering Sciences and Technology Division, CSIR-North East Institute of Science & Technology, Jorhat 785006, India.

E-mail addresses: [ingolepravin@gmail.com](mailto:ingolepravin@gmail.com), [pingole@neist.res.in](mailto:pingole@neist.res.in) (P.G. Ingole).

<sup>1</sup> Both authors contributed equally to this work.

<https://doi.org/10.1016/j.memsci.2020.118212>

Received 23 February 2020; Received in revised form 23 April 2020; Accepted 23 April 2020

Available online 7 May 2020

0376-7388/© 2020 Elsevier B.V. All rights reserved.

## 1. Introduction

The lack of potable water for human beings is increasing day by day, and almost whole world is facing a critical problem about clean and drinking water [1,2]. Conventional water purification technologies are energy consuming and not sufficient to provide clean potable water in bulk. Due to the eco-friendly nature of membrane technology, it is one of the best choice to fulfil demand for pure water requirement in large quantity. Therefore, the development of polymer membranes with steady performance is highly interested area of research in the separation and purification using membrane science and concern technologies [3]. Polymeric membranes are not only playing a key role in the purification of water, gas, pharmaceutically active molecules, etc. [4–6], but also an important role in our daily life [7,8]. There are several examples where polymeric membranes are acting as a main key barrier. Still now for water purification, there are several kinds of membranes are developed by several researcher like ceramic, zeolite, mixed matrix membranes (MMM), thin film composite (TFC), thin film nanocomposite (TFN) membranes etc. [9–16]. Recently in the development of nanofiltration (NF) membrane, the electrostatic and steric hindrance effect between the external solutions (feed solutions) and membrane are highly responsible factor to explaining the separation mechanism. Therefore, researcher focusing on the coating on NF membrane using different coating solutions, to get high separation against targeted feeds [17,18]. Removal of excess toxic boron from the water bodies by membrane technology is also a main task for the membrane researchers and various membranes have been developed for boron rejection [19]. As per the guideline by WHO only a 0.3 mg/L boron is permissible for the human body; excess boron is dangerous and make side effects on human health [19,20]. Boron intakes for plants and animals also varies in the range of 0.5–5.0 mg/L [21]. Recently, Hu et al. developed the sulfonated polyamide TFC membrane resulted 90.6% boron removal under a single reverse osmosis process [22]. The detail mechanistic study of boron removal from seawater was carried out by Hyung and Kim in their investigation they explained the model for performance prediction and design for sea water reverse osmosis processes [23]. In the case of humic acid rejection, it is important to develop antifouling membranes which also shows antibacterial properties. It's important to mention here that very less research work has been found on the antibacterial properties investigation by membrane application [24–27]. For the humic acid separation the membrane antifouling and antibacterial properties are very important prior to the chlorination process. The competitive adsorption of pharmaceuticals personal care products (PPCP) and humic substances by CNT membranes was applied by Wang et al. and reported that the CNT had played a very important role as an adsorbent for the removal of PPCP compounds from waste-water treatment [28]. In current work we considered alarming targeted pollutants and also focus to develop the TFN membrane with novel high efficient materials to achieve 99% or more than that rejection efficiency along with better bactericidal properties.

In water purification, mostly reverse osmosis (RO) membranes are applied. The performances of these membranes are high up to a certain level but after continuous use there is reduction in permeability results due to fouling problems [29,30]. Therefore, several methods are approaches by the researchers to reduce the fouling issues [31–33]. Current studies we too focused on the antifouling, low-cost, energy-saving and eco-friendly aspects in TFN membrane development for the purification of water. In NF membrane the separation of solute through the membrane is governed by a sieving mechanism (size exclusion phenomenon) and electrostatic interaction called the Donnan principle [34]. To resolve the fouling issues, the NF-TFN membranes are the best alternative for various applications [35]. In NF-TFN membrane, the chemistry tweaked to give the anticipated surface charge and high selectivity (rejection) during the membrane preparation process via interfacial polymerization while making the polyamide layer [36,37].

Development of TFN membranes using various nanoparticles like

SiO<sub>2</sub>, TiO<sub>2</sub>, Zeolite, CeO<sub>2</sub>, etc., were reported by the several researchers which shows the advantages like fouling resistance, enhanced flux and salt rejection [38–41]. Along with these nanoparticles from last half decades' researchers are concentrated on the preparation of MOF incorporated TFN membranes due to superior surface area, large pore volumes, and tuneable pore structures, which collectively advantageous to give high separation result with antifouling properties [42]. Zr-based UiO-66 family MOFs, due to high stability in aqueous medium are already successfully applied in the preparation of highly water-stable membranes for liquid separation [43]. As important analogues, amine functionalized UiO-66-NH<sub>2</sub> might provide a good scope for improving the compatibility between MOFs and polymers due to strong interfacial polymerization with free functional groups on MOF. Eventhough, sometimes the interaction of MOF particles and polymer species typically showed poor compatibility due to the easy agglomeration of MOF crystals, which consequently decrease in membrane efficiency [44]. Also their strong limitation due to high synthesis cost of MOFs in membrane development. Therefore, mentioned both issues (cost and agglomeration) can be overcome by synthesising MOF material in presence of suitable support material.

Mesoporous synthetic hectorite (MSH) is a distinctive speciality additive/support; a layered magnesium silicate layered material which properties and composition quite similar to natural hectorite clay mineral. MSH has a layered morphology which, can distribute in water in the form of disc shaped crystals. MSH types of synthetic materials are already playing key role to improve suspension stability and emulsion stability in different areas of industrial formulations. The details about innovative synthesis approaches, structural and textural properties results and applicability of the developed MSH in different areas already proved in our previous reports [45–48].

Here in present investigation for the first time MSH is selected as a choice support material for membrane modification due to negative surface charge, suitable structural/textural properties, surface hydroxyl functionalities, high dispersion and strong coating ability. Additionally, as per our knowledge for the first time we developed the thin film nanocomposite membranes by adding MSH and MSH@UiO-66-NH<sub>2</sub> nanoparticles in the aqueous phase monomer and crosslinked with TMC. The performance of TFC and TFN membranes have been tested for above discussed targeted feeds solutions by optimising different batch parameters. The effect of MSH and MSH@UiO-66-NH<sub>2</sub> nanoparticles on the polyamide layer and its bonding has been examined. It is found that due to hydroxyl and amine groups of MSH@UiO-66-NH<sub>2</sub> nanoparticles the crosslink density of the membrane increases, and increased cross-linked density accountable for the enhanced performance of TFN membranes. The pressure effect on membrane performance has been studied. All prepared membranes have been characterized using various physicochemical characterization techniques and from the observed results possible mechanism was investigated. We believe that our research finding might be helpful in understanding MSH and MSH@UiO-66-NH<sub>2</sub> nanoparticles interaction with the monomers while making TFN layer to enhanced pure water flux and rejection against targeted feed solutions.

## 2. Experimental

### 2.1. Materials

For the synthesis of MSH, Ludox HS-40 as a precursor source for 40%, stabilized silica solution (DuPont), magnesium chloride hexahydrate, lithium fluoride, sodium hydroxide, were procured from S.D. fine chemicals Ltd., Mumbai, India. For the synthesis of UiO66-NH<sub>2</sub> Zirconium(IV) chloride [ZrCl<sub>4</sub>, ≥97.0%], 2-Aminoterephthalic acid [MF/MW: C<sub>8</sub>H<sub>7</sub>NO<sub>4</sub>/181.15, Purity: >98.0%], Acetic acid [MF/MW: CH<sub>3</sub>COOH/60.05, purity: 99.7%]; *N,N*-dimethylformamide [MF/MW: HCON(CH<sub>3</sub>)<sub>2</sub>/73.09, purity: 99.7%]; Ethanol [MF/MW: C<sub>2</sub>H<sub>5</sub>OH/46.07, purity: 99.5%] were purchased from S.D. fine chemicals Ltd., Mumbai,

India. Polysulfone (PSf, MW = 30000) for the preparation of membrane support, piperazine (PIP) and trimesoyl chloride (TMC) for interfacial polymerization to make selective layer were received from M/s Sigma-Aldrich Chemical Company, USA. The solvent *N,N*-dimethyl formamide (DMF) were used to make homogeneous solution of DMF for preparing the support layer, *n*-hexane (99.9%) solvent for the preparation of TMC solution obtained from M/s RANKEM range of laboratory chemicals, Gujarat, India. For feed solutions NaCl, Na<sub>2</sub>SO<sub>4</sub>, CuSO<sub>4</sub>, MgSO<sub>4</sub>, MnSO<sub>4</sub>, purchased from S.D. Fine Chemicals Ltd., Mumbai, India and Boric acid, humic acid received from M/s Sigma-Aldrich chemical company, USA. Deionised (DI) water used for making PIP solution, obtained from millipore available in our lab at CSIR-NEIST. An adjustable casting knife was used for casting PSf support layer on the non-woven fabric. All chemicals were used as received.

## 2.2. Experimental

### 2.2.1. Preparation of MSH

MSH synthesis was carried out by adopting a previously reported methodology [49]. The required synthesis precursors were reacted in the molar ratios of LiF:MgO:SiO<sub>2</sub> = 0.266:1.00:1.52 respectively [45]. The freshly prepared magnesium hydroxide was added to an aqueous solution of lithium fluoride then the suspension was added to silica sol and mixed with a homogenizer for another 30 min at room temperature. The homogenised slurry was continuously stirred in reflux condition for 48 h. The obtained product was separated, thoroughly washed and dried in air circulated oven at 110 °C for 10 h and fine grinded product was kept in an air-tight bottle for further use.

### 2.2.2. Preparation of MSH@UiO-66-NH<sub>2</sub>

Synthesis of MSH@UiO-66-NH<sub>2</sub> was carried out by a microwave-assisted DMF solvent-based modulated solvothermal synthesis approach. In detail, synthesis procedure as-synthesized MSH exactly 280 mg was first dispersed well in 35 ml of dimethylformamide solvent in 100 ml of teflon microwave reactor by ultrasonication. Afterward, 320 mg of ZrCl<sub>4</sub> and 250 mg of 2-aminoterephthalic acid were dissolved in a well-dispersed prepared MSH solution. After complete mixing of MOF precursors, precisely 43.7 mmol of acetic acid was dropped into a reaction mixture as modulator and stirred for 15 min. Subsequently, the homogeneously synthesized solution was transferred into the microwave reactor and reacted under 1000 W of irradiation at 150 °C for 1 h. After cooling down to the room temperature, the resulted product was washed by using (10 ml x 3) of fresh DMF solvent and (10 ml x 4) with ethanol. Finally, the obtained solid residue was dried in an air-circulated oven at 150 °C for 12 h. The obtained product was designated as MSH@UiO-66-NH<sub>2</sub> and stored for further application.

## 2.3. Membrane preparation

### 2.3.1. Preparation of PSf membrane

The PSf membranes were fabricated by phase inversion technique. *N,N*-dimethylformamide is used as a solvent to make 18 wt% polysulfone homogeneous solution at 60–70 °C under continuous stirring. After preparing the homogeneous solution of polysulfone the polymer solution was evacuated to remove air bubbles and after that the polymer solutions used for the casting of PSf support membranes. The membranes are casted on a non-woven polyester fabric those are purchased from Filtration Sciences Corporation, USA under controlled relative humidity of 30–35% and temperature of 25–30 °C using doctor's blade. The prepared membranes were air exposed for 30 s before precipitation to de-ionised water containing DMF (2%) and sodium lauryl sulphates surfactants (0.1%). The membranes were taken out from the precipitation solution after 30 min and washed systematically with de-ionised water to remove the surfactant and solvent. The prepared membranes were stored in deionised water until next use.

### 2.3.2. Preparation of TFC and TFN membranes

The selective layer of composite and nanocomposite membrane was prepared on polysulfone support membrane by interfacial polymerization. To prepare thin film composite layer we used piperazine (PIP, 2 wt %) called aqueous phase monomer solution and trimesoyl chloride (TMC, 0.2 wt%) called organic phase monomer solution. For the development of TFN membranes we used MSH and MSH@UiO-66-NH<sub>2</sub> nanoparticles. To prepare hydrophilic TFN layer the polysulfone membrane first immersed in an aqueous solution of PIP containing nanoparticles (2 wt% PIP and 0.01 wt% nanoparticles) for 5 min. After 5 min the membrane was drained off for 5–10 min to remove additional solution. Subsequently, after complete removal of water droplets, it was immersed in *n*-hexane solution of TMC for 3 min. The prepared TFC and TFN membranes were consequently treated in oven under hot air circulation at 70–80 °C for 10 min for to attain chemical stability to polymer layer. The schematic representation of TFN membrane preparation is shown in Fig. 1. The TFC and TFN membranes preparation conditions are summarized in Table 1.

## 2.4. Material and membrane characterizations

The materials powder XRD pattern was recorded over a 2θ range of 0–70° using Rigaku, Ultima IV X-ray diffractometer. Attenuated Total Reflectance Fourier Transform Infrared (ATR-FTIR) is an analytical technique used to identify organic, inorganic and polymeric materials. This method uses infrared light to scan test samples and observe chemical properties. The frequency range measured as wave numbers typically over the range 4000–400 cm<sup>-1</sup> using PerkinElmer, System 2000 Infrared Spectrophotometer. XPS analysis using Thermo Fisher Scientific: ESCALAB Xi measure the elemental composition, empirical formula, chemical state and electronic state of the elements within a material. FESEM analysis was done using Carl ZEISS Microscopy, Germany instrument to obtain information about surface topography and composition. HR-TEM analysis was done using TEM-2100 Plus electron microscope. TGA is a method of thermal analysis in which changes of physical and chemical properties of materials are measured as a function of increasing temperatures using PERKIN Elmer PC series, DSC 7. AFM analysis was done using AFM/SPM instrument (Ntegra Aura Model NT-MDF, Moscow) in semi contact mode. Contact angle measurement (CA) was done using DM-501, Kyonea Interface Science based on sessile drop method using water as the probe liquid at temperature 25 °C. For humic acid to calculate rejection the absorbance was determined by UV-vis spectrophotometer, Specord 200. Zeta potential was done to find out the surface charge and its changes using SurPASS™ Electrokinetic Analyzer (Anton Paar, Austria).

## 2.5. Membrane performance experiments

The prepared membranes performances were evaluated by the cross-flow NF/RO membrane testing instrument provided by M/s. Prova Pvt. Ltd. Mumbai, India as shown in Fig. S1. The test of different salts/acids rejection was done using different feed model solutions i.e. Na<sub>2</sub>SO<sub>4</sub>, MgSO<sub>4</sub>, CaSO<sub>4</sub>, MnSO<sub>4</sub>, NaCl, boric acid and humic acid for the experiments. Except humic acid (1000 mg/L) each feed solution concentration maintain to 2000 mg/L in DI water. Same like above mentioned salts the humic acid 1000 mg/L is also tested using same membranes. The cross-flow membrane test was done using 1.5 MPa *trans*-membrane pressure with feed flow 4 L/min at room temperature. To avoid any uninvited hydraulic resistance before start salt rejection experiments the all prepared membranes were compacted by cross-flow of DI water for 2 h under ideal experimental conditions. The rejection of salt is calculated using conductivity meter from the calibration curve. UV spectrophotometer is used for humic acid rejection and boron calculations (for boron calculation Hach Carmine Method is used). The following equations (1) and (2) are used to calculate flux and salt rejections.

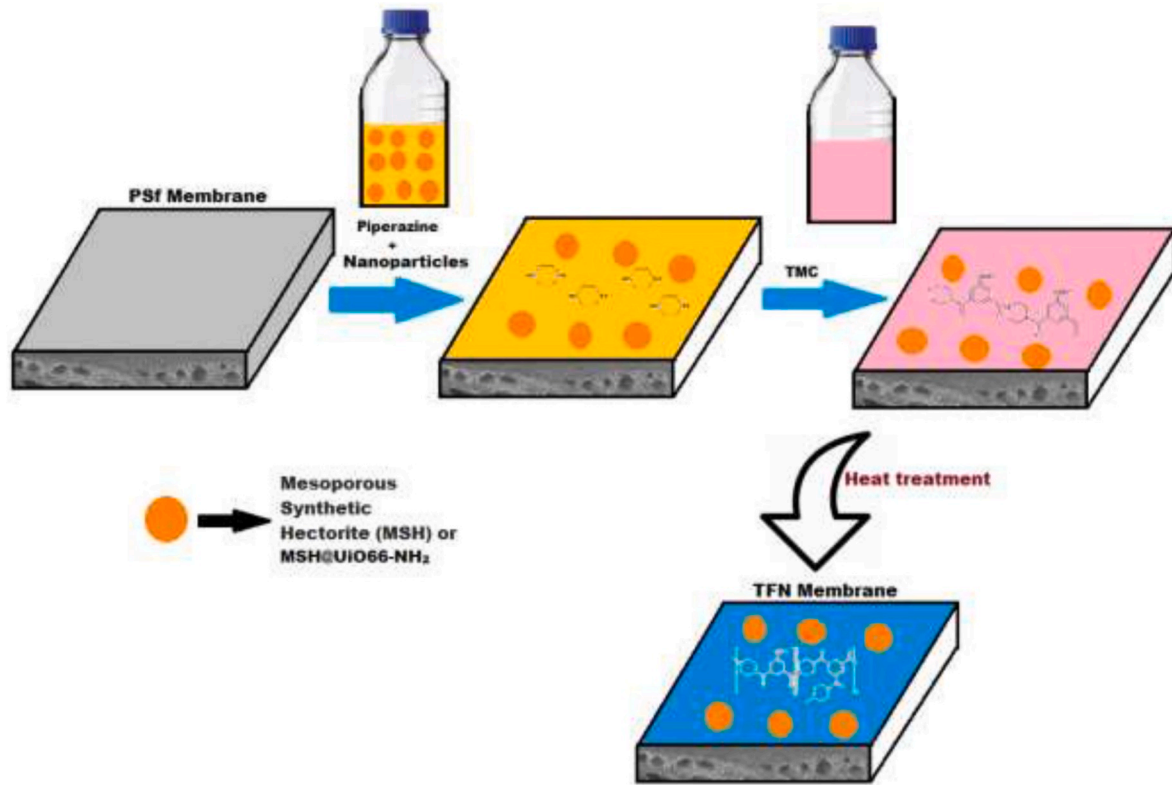


Fig. 1. The graphic illustrations of thin film nanocomposite membrane preparation along with polyamide cross-linked structure on the surface of polysulfone membrane.

Table 1

Composition of aqueous (NPs + PIP) and non-aqueous (TMC) solutions and reaction times for interfacial polymerization.

Membrane Name	PIP Conc. (wt %)	NPs Conc. (wt %)	TMC Conc. (wt %)	Reaction time (min)
PT-TFC	2.0	0.0	0.2	3
MSH-TFN	2.0	0.01	0.2	3
MSH@UiO-66-NH <sub>2</sub> -TFN	2.0	0.01	0.2	3

$$J = \frac{V_f}{A \times \Delta t} \quad (1)$$

where,  $J$  is water flux,  $V_f$  is the volume of the filtrate flow,  $A$  is effective membrane area and  $\Delta t$  is the time intervals.

Salt rejection is calculated by using equation (2).

$$R = 1 - \frac{C_p}{C_f} \times 100 \quad (2)$$

where  $C_p$  and  $C_f$  are the concentration of permeate and feed respectively.

To analyse the transport process of boron, using Eq. (3) is used (here the permeability coefficients [ $B_s$ ] of boron through the membranes were evaluated).

$$J_s = B_s \times \Delta C_s \quad (3)$$

Where  $J_s$  represent the permeation flux and  $B_s$  represent as a coefficient of the boron, and  $\Delta C_s$  represent the concentration difference between the feed and permeate.

Humic acid retention is determined using the following equation (4)

$$R_h = 1 - \frac{C_{hp}}{C_{hf}} \times 100 \quad (4)$$

where  $C_{hp}$  and  $C_{hf}$  are the humic acid concentrations in the permeate solution and feed solution respectively.

## 2.6. Antibacterial test of MSH@UiO-66-NH<sub>2</sub>-TFN membrane

The plate colony-forming unit (CFU) count method is used for the antibacterial activity test of targeted membrane. Here MSH@UiO-66-NH<sub>2</sub>-TFN membrane was cut in an ideal portion and sterilised using 70% ethanol solution and by exposing in UV light. Furthermore, the culture of *E. coli* BI21 (*Escherichia coli*) with  $3 \times 10^5$  CFU/ml was used for incubation of membrane for 4 h at 37 °C using rotatory shaker at 300 rpm. After that the resultant solution were diluted and 100  $\mu$ L diluted solution were inoculated on agar plates followed by an overnight incubation at same temperature (37 °C). Then sterilised membrane cuts were tested in the bacterial environment, for the CFU counting  $10^{-6}$  dilution plate method was used.

## 3. Results and discussions

### 3.1. Nanoparticles characterizations

Fig. 2a shows PXRD patterns of MSH, and MSH@UiO-66-NH<sub>2</sub> showed major peaks at 11.2, 4.5, 3.15, 2.56 and 1.52 Å correspond to (001), (110, 020), (130, 200), and (060, 330) planes of hectorite clay respectively. However, in the MSH diffraction plot, no peaks were observed at  $2\theta = 4.77$  and  $22.8^\circ$  which are corresponding to the magnesium hydroxide mineral and amorphous silica respectively; this confirms that in the material synthesis process original  $Mg(OH)_2$  and silica have been converted to MSH phases [50,51]. Moreover, the MSH showed '001' reflection distance 11.2 Å, ( $2\theta = 4.98^\circ$ ) which is found in the range of 9.6–14 Å confirms the characteristics layered smectite clay minerals [52]. Whereas, the PXRD pattern of MSH@UiO-66-NH<sub>2</sub> showed characteristics peaks of both nanomaterials (MSH and



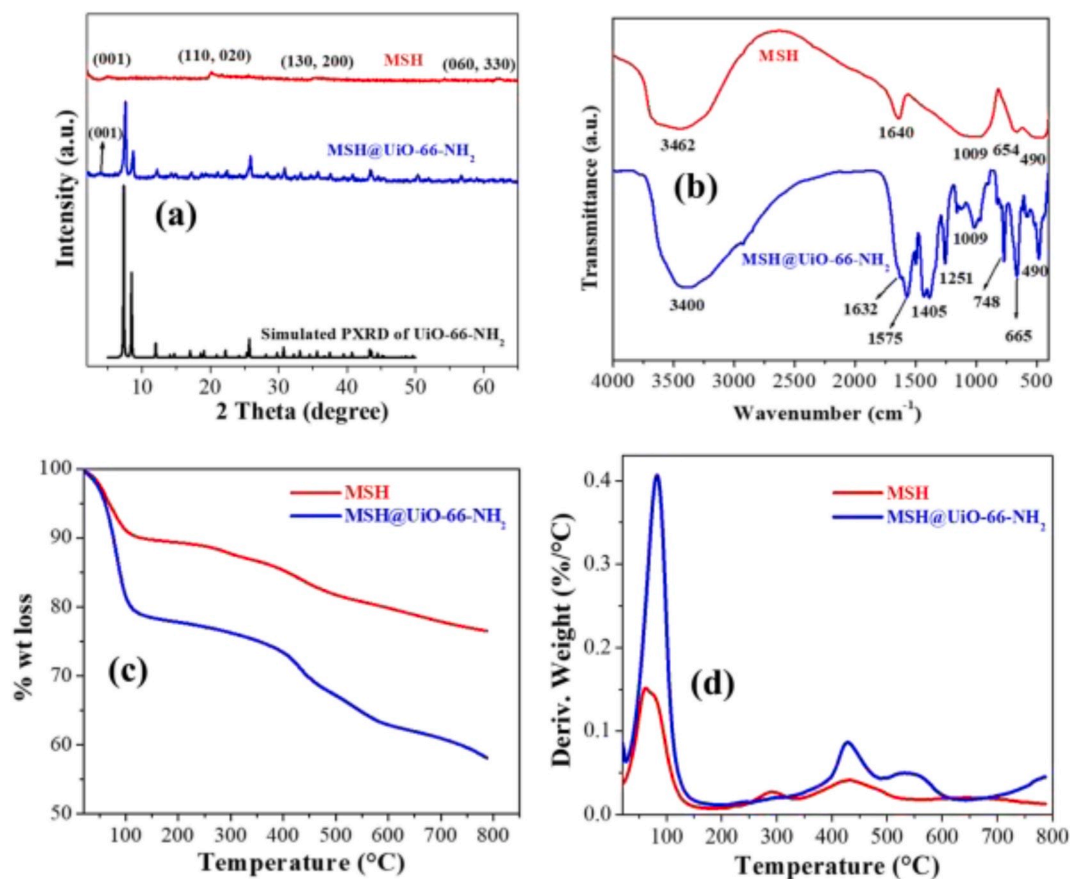


Fig. 2. (a) Powder X-Ray diffraction patterns of MSH, MSH@UiO-66-NH<sub>2</sub> and simulated Zr-UiO66-NH<sub>2</sub>, (b) FT-IR spectra of MSH and MSH@UiO-66-NH<sub>2</sub> nanoparticles, (c) TGA and (d) DSC thermographs of MSH and MSH@UiO-66-NH<sub>2</sub> nanoparticles.

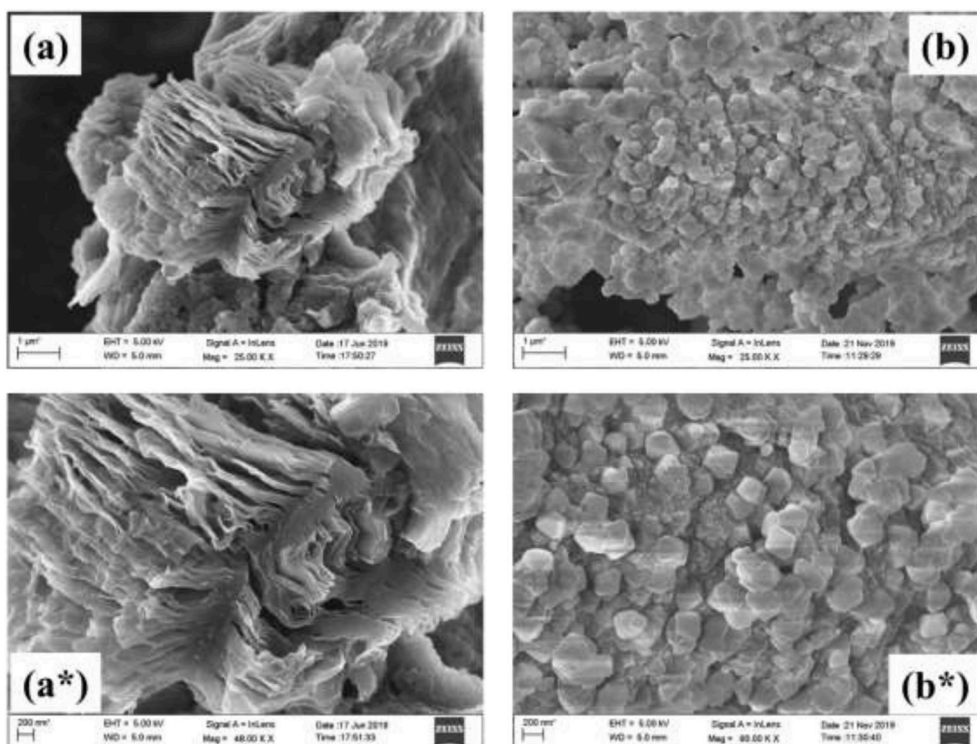


Fig. 3. SEM images for (a and a\*) MSH and (b and b\*) MSH@UiO-66-NH<sub>2</sub> nanoparticles.

UiO-66-NH<sub>2</sub>). In case of composite MSH d(001) peaks shifted to lower angle  $2\theta$  from 4.98 to 3.9° indicates intergallery expansion of MSH confirms the intercalation of MOF species on MSH. Also PXRD composite patterns exactly matched well with simulated XRD pattern of UiO-66, family MOFs confirms the successful formation of highly crystalline Zr-UiO66-NH<sub>2</sub> MOFs nanoparticles in the composite [53].

The FTIR spectra of synthetic MSH and MSH@UiO-66-NH<sub>2</sub> are displayed in Fig. 2b, the MSH spectra evidently shows the Si-O stretching and in-plane bending spectra at 1009 cm<sup>-1</sup>. However, spectra observed at 3462 and 1640 cm<sup>-1</sup> were allied with the Mg(OH) stretching and bending vibrations individually whereas, the Mg-O bending vibrations contributed a low-intensity band at 654 cm<sup>-1</sup> [48]. The new band formed during MSH@UiO-66-NH<sub>2</sub> synthesis at 490 cm<sup>-1</sup> attributed to Zr-O bond [54]. The characteristics peaks at 748 cm<sup>-1</sup>, 665 cm<sup>-1</sup> attributed to C-N, C-H group respectively [55]. In MSH@UiO-66-NH<sub>2</sub> due to -COOH group in 2-Aminoterephthalic acid as an organic ligand the additional two strong -CO coupling peaks are observed at 1575 cm<sup>-1</sup>, and 1405 cm<sup>-1</sup> belongs to symmetric and asymmetric stretching vibration peaks respectively [56]. Fig. 2c and d represent the TGA and DSC curves of as synthesized MSH and MSH@UiO-66-NH<sub>2</sub>, here two distinct weight loss was found during thermal decomposition from 150 to 450 °C, before 150 °C is due to solvent or water loss. This weight loss after 200 °C was due to organic ligand 2-aminoterephthalic acid decomposition [57]. The remaining residue at the end of decomposition was observed due to Zr-O and comes from the MSH@UiO-66 [58]. The morphology of the as-synthesized MSH and MSH@UiO-66-NH<sub>2</sub> are presented in Fig. 3, MSH image showed a characteristic layered morphology similar like natural 2:1 smectite clay minerals [59]. Similar type of the layered stacks of MSH was also confirmed in previous report [45]. Whereas MSH@UiO66-NH<sub>2</sub> composite showed characteristics octahedral shaped crystals of UiO-66-NH<sub>2</sub> formed on the surface of MSH.

### 3.2. TFC and TFN membranes characterizations

#### 3.2.1. ATR-FTIR and XPS

The physiochemical properties of prepared membranes were characterized by ATR-FTIR analysis. The ATR-FTIR spectra of all membrane are shown in Fig. 4 and it has been found that all characterised TFN membranes containing the nanoparticles and these nanoparticles are closely bind with polyamide. It is also concluded that the nanoparticles have taken part in interfacial polymerization (due to active functional groups), so they are covalently bonded with selective layer. The common peak of PSf membranes i.e. 1150 cm<sup>-1</sup>, 1245 cm<sup>-1</sup>, and 1584 cm<sup>-1</sup> are characteristics of the sulfone group, and bands in the range of 850 cm<sup>-1</sup> – 1020 cm<sup>-1</sup> are for C-H stretching of aromatic ring of polysulfone were found [60]. The reduced intensity of these peaks in TFN membranes specifies the existence of very thin selective polymer layer on PSf membrane.

The characteristics peak of polyamide layer was observed at 1665 cm<sup>-1</sup> (C=O) stretching vibration peak, the imide peak at 1772 cm<sup>-1</sup> (carboxyl C=O, due to oxidized -COCl group to -COOH group of TMC), and peaks at 1546 cm<sup>-1</sup> correspond to amide -NH bending vibration peak were observed. Also the peaks at 1372 cm<sup>-1</sup> (C-N-C, imide in the plane), and 751 cm<sup>-1</sup> (C-N-C, out-of-plane bending, imide) was observed. More than this the presence of MSH, and MSH@UiO-66-NH<sub>2</sub> nanoparticles in the membranes also confirmed by 3462 and 1640 cm<sup>-1</sup> were allied with the Mg(OH) stretching and bending vibrations the peaks came from MSH, whereas, the additional -CO peak from the used MOF was observed at 1401 cm<sup>-1</sup> in MSH@UiO-66-NH<sub>2</sub>-TFN membrane [61].

XPS analysis of all prepared membranes were done to find the chemical composition in the selective polyamide layer. The chemical composition was found changed in TFN membranes after adding various kinds of nanoparticles. The chemical bonding information of C, N, O atoms were obtained by deconvoluting high resolution XPS spectra. Fig. 5 shows the high resolution XPS scans of C (1s), O (1s) and N (1s). The main changes are observed for peaks of C (1s) in PT-TFC, MSH-TFN,

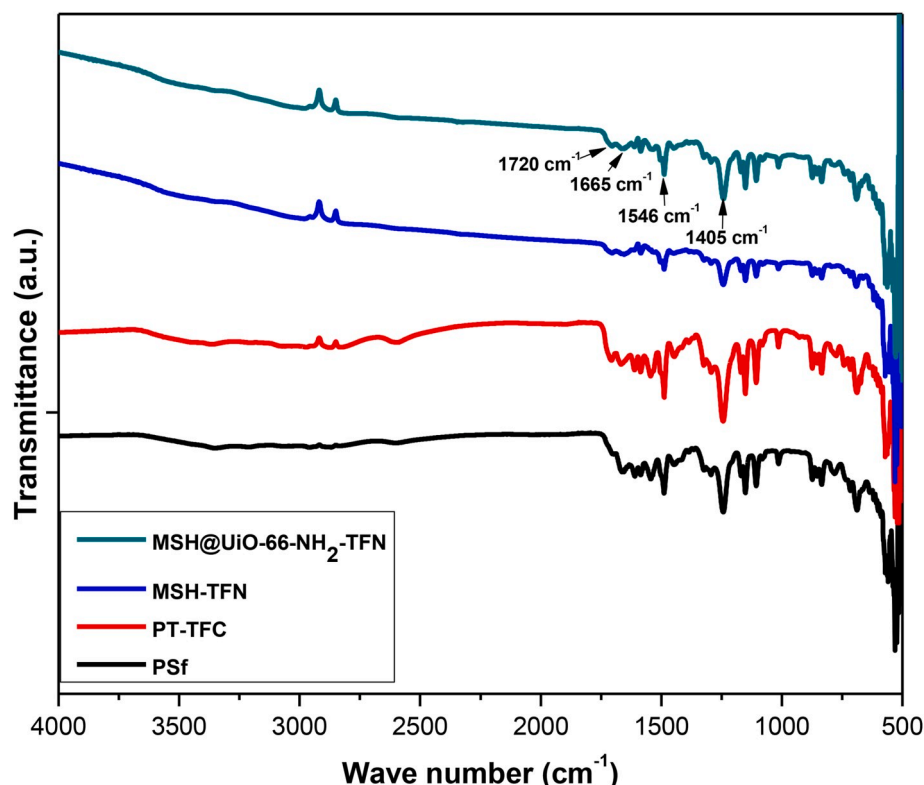
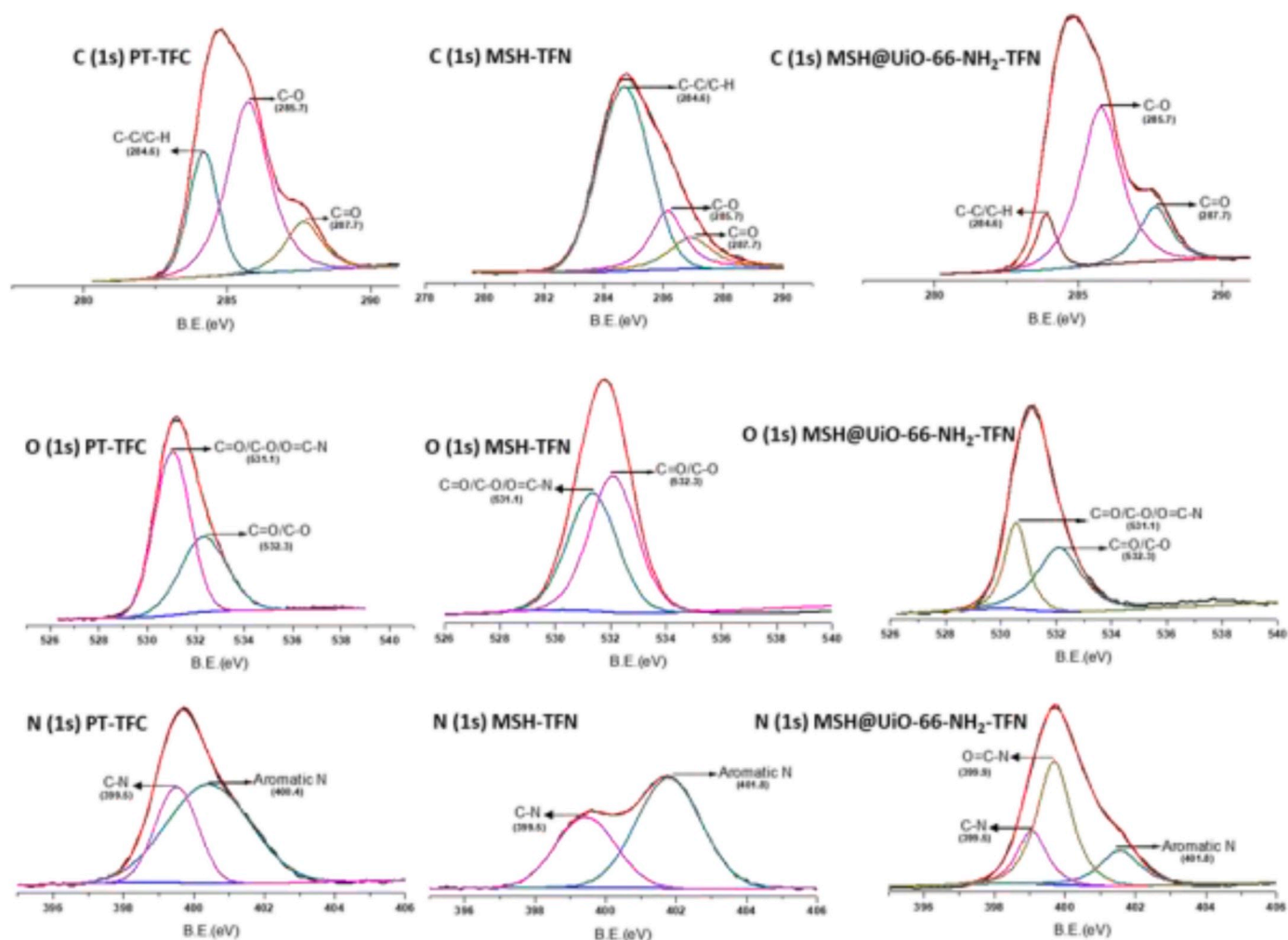


Fig. 4. ATR-FTIR spectra of (a) PSf, (b) PT-TFC, (c) MSH-TFN and (d) MSH@UiO-66-NH<sub>2</sub>-TFN membranes.



**Fig. 5.** High-resolution XPS spectra and peak deconvolution of C (1s), O (1s), and N (1s) of (a) PT-TFC, (b) MSH-TFN and (c) MSH@UiO-66-NH<sub>2</sub>-TFN polyamide based membranes.

and MSH@UiO-66-NH<sub>2</sub>-TFN polyamide based membranes.

In all prepared membrane the major peak at 284.6 eV ( $\delta_{BE} = 0$ ) is assigned to carbon atoms either C-C bond or C-H bonds. The peaks observed around 285.7 eV which is due to the carbon atom bonded with oxygen (C-O) group. Another small peak around 287.7 eV is observed due to O=C-O in carboxyl and O=C-N in the amide group [62]. The formation of obtained structure and functional groups are also confirmed by ATR-FTIR (Fig. 4). Furthermore, the other two more peaks carbonyl oxygen (O=C-O, O=C-N) at 531.1 eV and carboxyl oxygen (O=C-O) at 532.3 eV are observed. The XPS peak at 399.5 eV is observed in all prepared membranes due to amide nitrogen in TFC and TFN membranes. The aromatic nitrogen peak also observed at 401.8 eV, which is a result of contributions from piperazine. The union of FTIR and XPS analysis engrained the effective incorporation of the MSH, and MSH@UiO-66-NH<sub>2</sub> nanoparticles in the membranes. The elemental atomic wt% analysis of all prepared membranes along with PSf substrate

have been added in Table 2.

### 3.2.2. FE-SEM study for surface and cross-section morphology

The surface and cross-section morphology of TFC and TFN membranes are shown in Fig. 6. The PSf membrane surface and cross-section images are shown in Fig. S2. It is clearly seen that in the TFN membranes, both types of nanoparticles are well dispersed, predominantly MSH@UiO-66-NH<sub>2</sub> nanoparticles incorporated TFN membranes are uniformly dispersed on the membrane surface. The high-resolution images of all membranes are shown in Fig. 6. To see the comparative differences, the prepared membranes the cross-sections were investigated, appreciable differences have been found in cross-section images. The cross-section image of PT-TFC, MSH-TFN and MSH@UiO-66-NH<sub>2</sub>-TFN membranes shown the very thin selective layer containing nanoparticles on the surface of TFN membranes. MSH incorporated both TFN membranes cross-section image shows that due to the large particle size of

**Table 2**

Elemental analysis of PSf, TFC and TFN membranes by XPS.

Membranes	C (%)	O (%)	N (%)	Li (%)	Si (%)	S (%)	Zr (%)	Na (%)	Mg (%)
PSf	78.56	18.19	ND	ND	ND	3.26	ND	ND	ND
PT-TFC	69.08	16.46	11.67	ND	ND	2.79	ND	ND	ND
MSH-TFN	67.91	14.06	11.74	0.58	1.91	2.06	ND	0.66	1.09
MSH@UiO-66-NH <sub>2</sub> -TFN	68.8	15.66	11.84	0.27	1.11	1.37	0.16	0.34	0.48

(ND stand for Not Detected in XPS analysis).



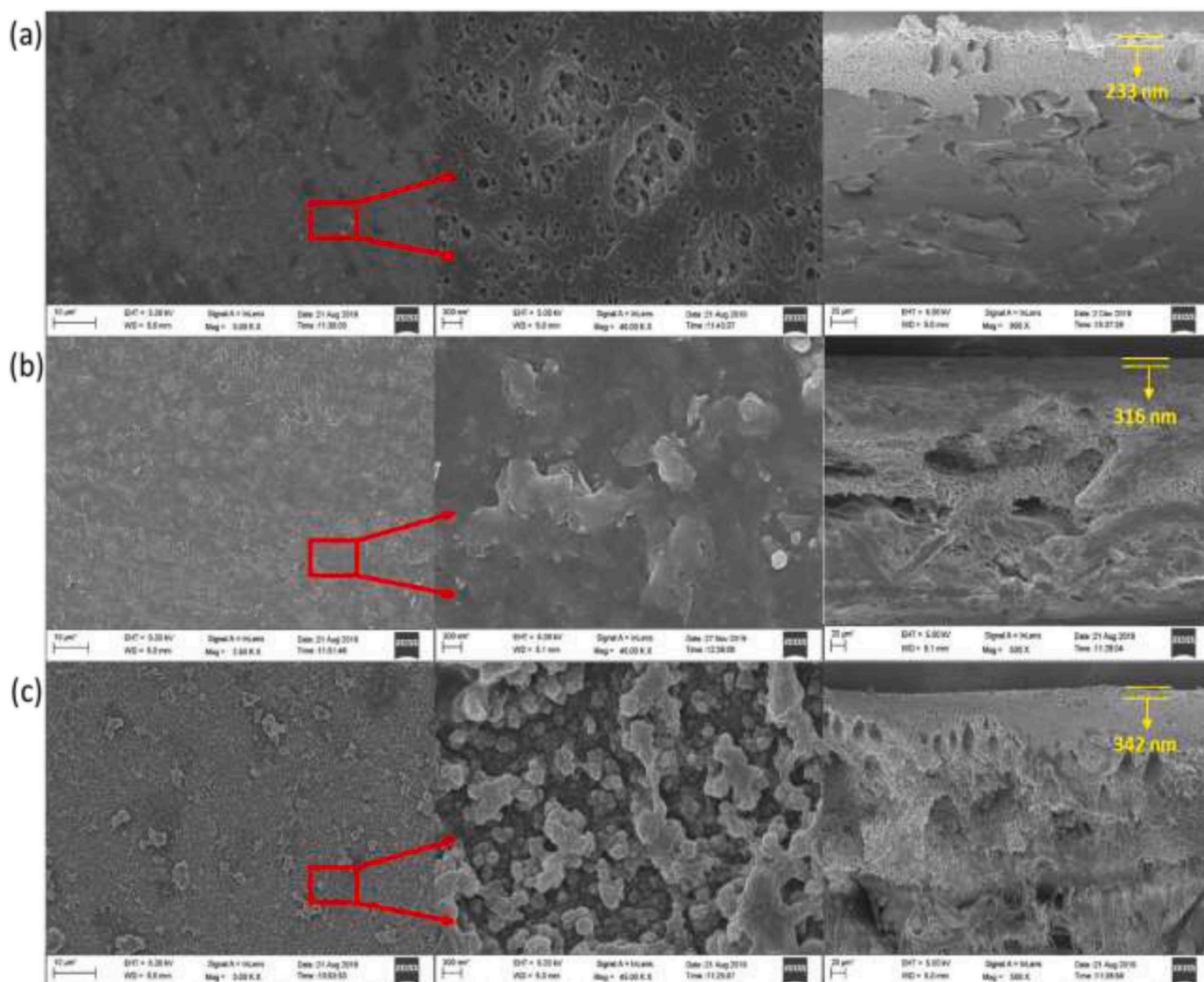


Fig. 6. FE-SEM images of surface and cross-section of (a) PT-TFC, (b) MSH-TFN and (c) MSH@UiO-66-NH<sub>2</sub>-TFN membranes.

nanoparticles comparatively thick selective layer formed. In both MSH-TFN and MSH@UiO-66-NH<sub>2</sub>-TFN membranes, the nanoparticles are covalently bonded with polyamide layer due to hydroxyl and amine functional groups on the nanoparticles. There are no defects are found due to electrostatic interaction between the aqueous phase monomer and polymer substrate and it designating that the good interfacial compatibility. It is also found that PT-TFC membrane thickness is less than the TFN membranes as marked in Fig. 6. The average selective layer thickness was observed in the range of 200–350 nm. The measured thicknesses are totally based on SEM images.

### 3.3. AFM

Nanoparticles were used to modify membrane properties to improve the performance of membranes and reduce the fouling issue. It is well know that the fouling has been shown related to membrane surface roughness in NF membrane process [63]. The use of nanoparticles for developing TFN membranes permits two things one is a high degree of fouling control and other is capability to produce anticipated membrane structure. Fig. 7 shows the 2D and 3D AFM images of PSf and all modified membranes. Atomic force microscopy was used to check the surface roughness of prepared membranes along with virgin membrane.

In this present work we found that nanoparticles added TFN membranes are showing antifouling characteristics. In modified membranes higher surface roughness controlled two major changes i.e. enhanced the antifouling performance and increasing the efficient filtration area. Because due to porous nature of nanoparticles water molecules can permeate fast through them and achieve enhanced flux [64].

As shown in Fig. 7 the 'valley-ridge' structure was clearly appeared and the surface roughness 9.67 nm for PSf, 44.2 nm for PT-TFC, 47.8 nm for MSH-TFN, and 52.3 nm for MSH@UiO-66-NH<sub>2</sub>-TFN membranes were observed. In all modified (TFC & TFN) membranes, comparatively highly rougher surfaces were found than the PSf membrane. Interestingly the MSH@UiO-66-NH<sub>2</sub>-TFN membrane displayed the rough surface attributed to the attention of the TFN membrane surface by the leaf-like structure. Its confirm here that due to rough surface, the contact angles values of membrane goes lower so ultimately, the hydrophilicity nature of the modified membrane was increased consequently resulted in the superior flux performances.

The dark bright regions in the images reconfirm the strong interaction between applied nanoparticles and polymer matrix functionalities. Compare with TFC, the TFN membranes shows the enhancement in all parameters (i.e. root mean square roughness ( $R_q$ ), average roughness ( $R_a$ ), and roughness max ( $R_{max}$ )). Additionally, in case of MSH@UiO-66-



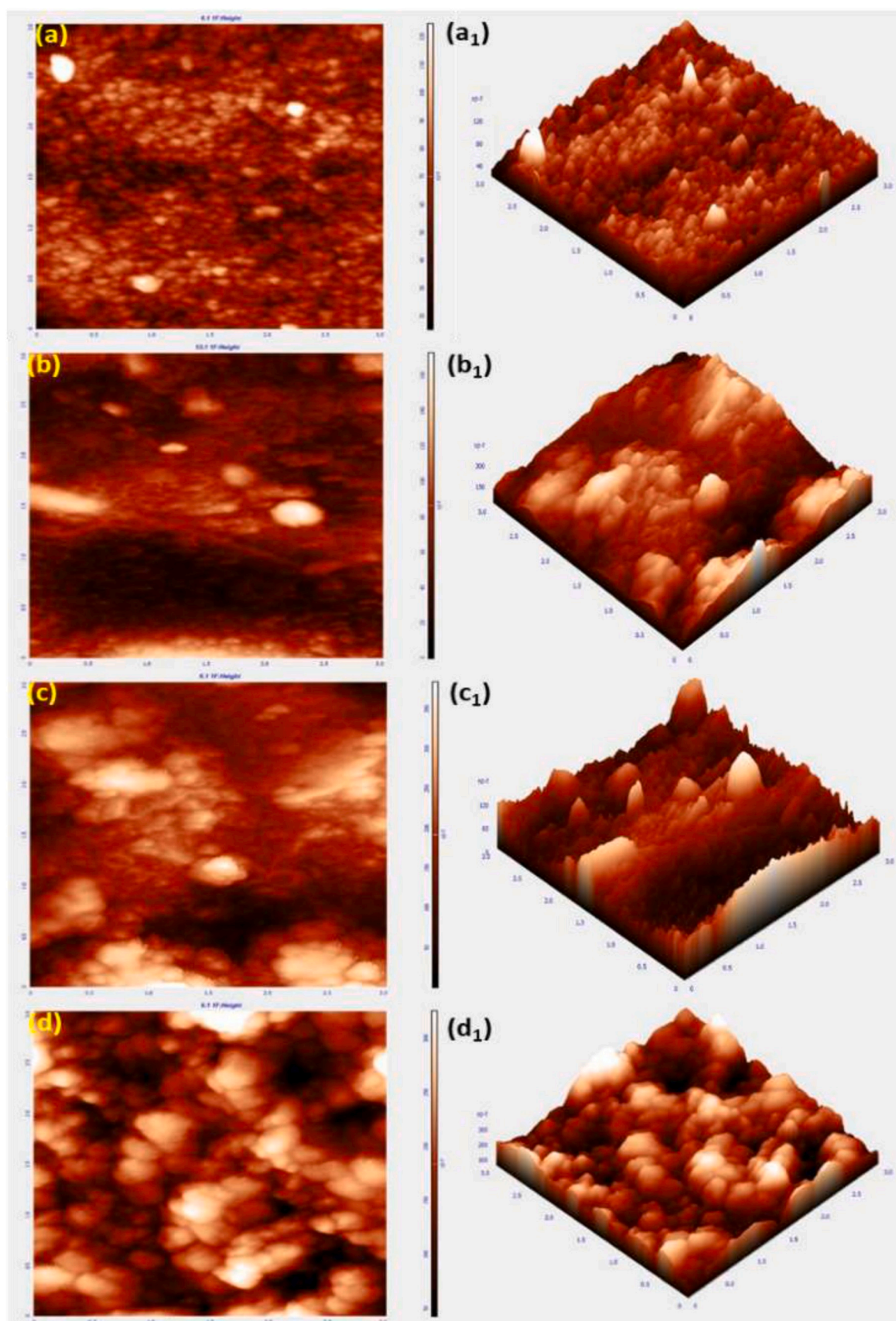


**Fig. 7.** Surface morphology of (a,a<sub>1</sub>) PSf, (b,b<sub>1</sub>) PT-TFC, (c,c<sub>1</sub>) MSH-TFN and (d,d<sub>1</sub>) MSH@UiO-66-NH<sub>2</sub>-TFN membranes envisaged via AFM.

NH<sub>2</sub>-TFN membrane, it is also probable that the free amine and hydroxyl groups of MSH@UiO-66-NH<sub>2</sub> can interact with carbonyl chloride groups of the TMC by interfacial polymerization reaction; this might be one of the explanation for the observed surface roughness. As the results are shown in Table 3 it is concluded that an increase in the surface of PT-TFC, MSH-TFN, and MSH@UiO-66-NH<sub>2</sub>-TFN membranes compare with PSf due to increasing diffusion of piperazine molecules to the organic front where the reaction occurs robustly to form a rough surface.

### 3.3.1. Contact angle

Table 4 represent the contact angle values and images of PSf and prepared TFC and TFN membranes after adding MSH and MSH@UiO-66-NH<sub>2</sub> nanoparticles. It is clearly seen from the observed deformed shapes of droplets the contact angle value decreased from 89.1° (PSf) to 34.2° for MSH@UiO-66-NH<sub>2</sub>-TFN membranes. The contact angle for PT-TFC membrane was observed 53.2°. As the nanoparticles changed from MSH to MSH@UiO-66-NH<sub>2</sub> the contact angle reduced from 43.4° to 34.2°. It's clear here that due to textural properties difference and presence of functional groups represent the strong interaction and the higher surface roughness of TFN membranes generate superior hydrophilicity which consequently influence the high record performances of flux and rejection against different feed solutions. The contact angle of MSH@UiO-66-NH<sub>2</sub>-TFN membrane (34.2°) is comparatively 35.72% less than PT-TFC membrane (53.2°), it is due to more hydrophilicity of TFN membrane resulted in the better wetting ability of TFN membranes resulted fast transportation of water molecules through membrane [65]. It is also important to mention here that after interaction of used nanoparticles the membranes not only improved the surface hydrophilicity but also improved the pore hydrophilicity responsible for the size exclusion separation of applied feeds.

As a result, due to more hydrophilic surface the humic acid rejection and flux achieved very high. The reason is the more hydrophilic surface repel the hydrophobic foulant as already reported by Wai et al. [66].

### 3.3.2. HR-TEM

The high resolution TEM images of all prepared membranes are shown in Fig. 8. It is clearly distinguished from the TEM images the presence or absence of nanoparticles on the membrane layer. In MSH-TFN membrane the trivial agglomeration of characteristics layered nanoparticles are found, whereas in MSH@UiO-66-NH<sub>2</sub>-TFN membrane the nanoparticles are fully dispersed on the MSH or in between the layer of MSH with characteristics MOF crystals. Furthermore, it is also found that after adding nanoparticles in TFN layer the polyamide layer can play an improving role for the transport of water molecules along with enhanced rejection of targeted feed.

### 3.3.3. Zeta potential

Zeta potential technique is also used to characterize the different nanoparticles incorporated TFN membranes to check the surface functionality, stability of dispersed nanoparticles in TFN layer along with the interaction of added particles with solid polymer surface. The stability of nanoparticles is measured in terms of zeta potential. The zeta potential of TFN membrane is found in reduced order form PSf > PT-TFC > MSH-TFN > MSH@UiO-66-NH<sub>2</sub>-TFN membranes. The negative value of zeta potential in all membranes are ascribed to the negative charge from dissociation of functionalized nanoparticles [67]. Thin film composite

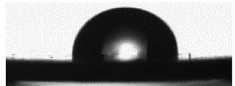
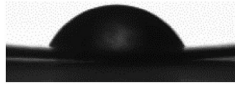


**Table 3**

Analytical statistics of surface roughness obtained by AFM analysis of PSf, PT-TFC, MSH-TFN and MSH@UiO-66-NH<sub>2</sub>-TFN membranes.

Membranes	R <sub>q</sub> (nm)	R <sub>a</sub> (nm)	R <sub>max</sub> (nm)
PSf	13.0	9.67	105
PT-TFC	51.5	44.2	130
MSH-TFN	59.6	47.8	221
MSH@UiO-66-NH <sub>2</sub> -TFN	66.0	52.3	355

**Table 4**

Contact angle (a) PSf, (b) PT-TFC, (c) MSH-TFN and (d) MSH@UiO-66-NH<sub>2</sub>-TFN membranes.

Membranes	Contact angle (°)	Image
PSf	89.1 (±2°)	
PT-TFC	53.2 (±2°)	
MSH-TFN	43.4 (±2°)	
MSH@UiO-66-NH <sub>2</sub> -TFN	34.2 (±2°)	

membranes are negatively charge (in the range pH 3.0–10.0) because of the hydrolysis of –COCl group of TMC to –COOH group. The TFN membranes are more negatively charge compare to TFC membrane. The zeta potential value for PT-TFC had –25.25 mV, MSH-TFN membrane had –33.86 mV, and MSH@UiO-66-NH<sub>2</sub>-TFN had –38 mV respectively. It is also found that more hydrophilic membrane has more negatively charge surface.

### 3.3.4. TGA

PT-TFC, MSH-TFN and MSH@UiO-66-NH<sub>2</sub>-TFN membranes were characterized using TGA analysis as shown in Fig. 9. The thermal stability of these membranes checked after coating of thin selective layer. Considerable variation is found in thermal properties of TFN membranes. As shown in Fig. 9 there are major three weight losses were found. The gradual weight loss is found for all TFC/TFN membranes, and first weight loss found in the temperature range 50–200 °C due to evaporation of water and the volatile matter. Second weight loss was observed in middle decomposition in the range 300–490 °C for all membrane for the polymeric decomposition and third weight loss found above 500 °C for aromatic and metallic decomposition in TFC/TFN membranes. It is also noted that nanoparticles slightly reduce the decomposition of TFN membranes [68] due to decomposition of ligand from the MOF that lies within (300–530 °C). As this results the final decomposition shifted from 400 °C to 600 °C due to the reason of presence of MSH nanoparticles in TFN membranes. Incorporation of nanoparticles in TFN membranes increases the thermal stability of the membranes.

### 3.4. Performance of TFC and TFN membranes

To examine the developed nanofiltration membranes, two main parameters are need to check, that are permeated flux and rejection by using different experimental conditions. In this work three types of membranes are considered and all these prepared membranes showed the benchmark flux. Fig. 10 (a) shows the permeability results and Fig. 10 (b) shows the feeds rejection results of all prepared membranes. The highest flux results were achieved through PT-TFC membrane at 2000 ppm common metal salts and other feed solutions as, Na<sub>2</sub>SO<sub>4</sub>: 118.8 L/m<sup>2</sup>.h, MgSO<sub>4</sub>: 47.0 L/m<sup>2</sup>.h, MnSO<sub>4</sub>: 54.8 L/m<sup>2</sup>.h, CuSO<sub>4</sub>: 75.4 L/m<sup>2</sup>.h, NaCl: 127.5 L/m<sup>2</sup>.h, boric acid: 94.6 L/m<sup>2</sup>.h. Whereas, for humic acid 86.9 L/m<sup>2</sup>.h flux results was observed at 1000 ppm initial concentration solution at pressure 1.5 MPa. The performance of the PT-TFC, MSH-TFN, and MSH@UiO-66-NH<sub>2</sub>-TFN have been also checked using above mentioned different types of feed solutions including common metal salts and acid in water. As shown in Fig. 10 (a) even though, PT-TFC membrane performance were found very high in the form of flux but nanoparticles incorporated MSH-TFN, and MSH@UiO-



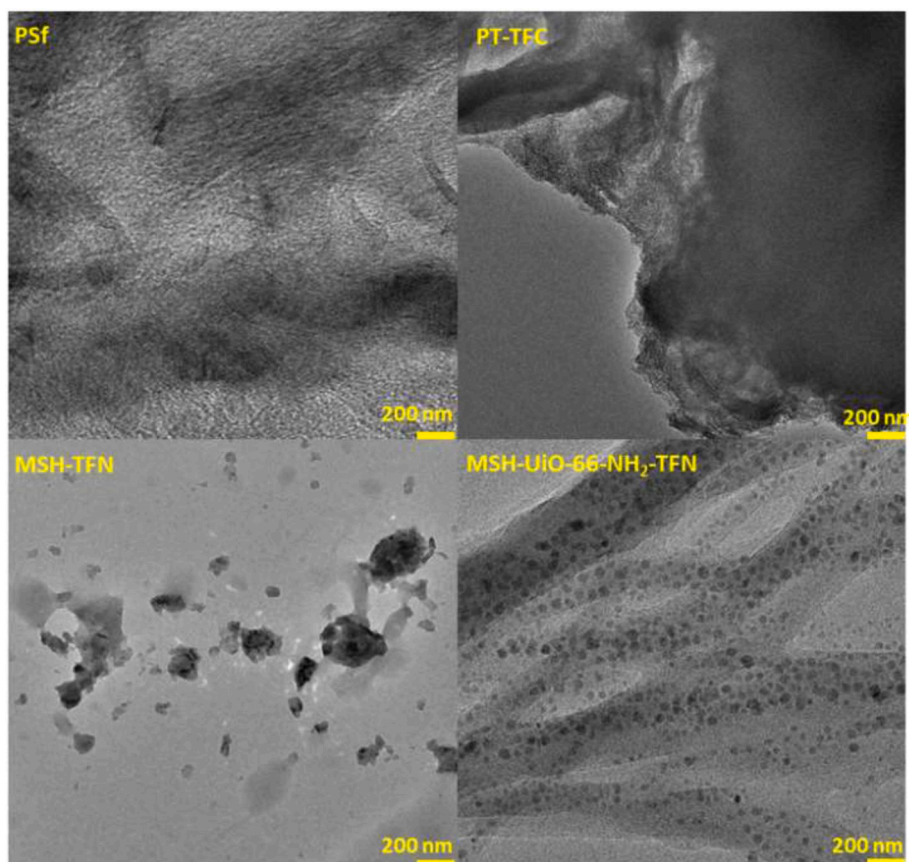


Fig. 8. TEM surface images of PSf, PT-TFC, MSH-TFN and MSH@UiO-66-NH<sub>2</sub>-TFN membranes.

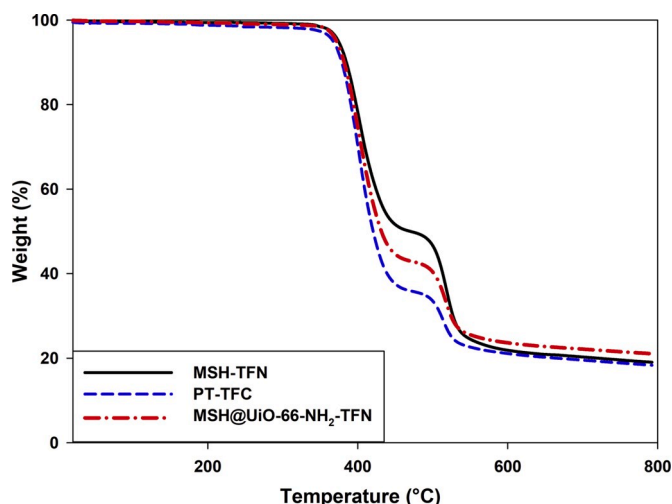


Fig. 9. TGA of PT-TFC, MSH-TFN and MSH@UiO-66-NH<sub>2</sub>-TFN membranes.

66-NH<sub>2</sub>-TFN were shows very high performance in the form of rejection with little sacrifice in the flux. At primary stage of experiments, we found that TFN membranes shows antifouling characteristic so we continued to comparative check with TFC membrane against applied feeds. On the basis of analysis of obtained results it was confirmed that the synthesized nanoparticles have taken part in the interfacial polymerization to avoid the leaching problem and it may also acme the boosted charge exclusion mechanism by the more negatively charged surfaces of TFN membranes (as found by zeta potential). It is noteworthy to mention that it's our first attempt to apply developed MSH and UiO-

66-NH<sub>2</sub> based composite nanomaterials to develop the membranes for above mentioned metal salts and humic acid solutions treatment. Interestingly rejection rate of MSH-TFN against all applied feed solutions was observed enhanced and also comparatively higher than TFC membrane. Considering these results MSH might be employable in different aspects of membrane development. As a results of rejection for focused MSH@UiO-66-NH<sub>2</sub>-TFN membrane was observed superior than all developed membranes. Particularly results of flux and rejection for different feeds are found like 94.0 L/m<sup>2</sup>.h flux with 82.29% rejection for 2000 ppm solution of Na<sub>2</sub>SO<sub>4</sub>, 34.78 L/m<sup>2</sup>.h flux with 94.42% rejection for 2000 ppm solution of MgSO<sub>4</sub>, 34.7 L/m<sup>2</sup>.h flux with 81.06% rejection for 2000 ppm solution of MnSO<sub>4</sub>, 60.86 L/m<sup>2</sup>.h flux with 84.62% rejection for 2000 ppm solution of CuSO<sub>4</sub>, 115.94 L/m<sup>2</sup>.h flux with 36.42% rejection for 2000 ppm solution of NaCl, 69.56 L/m<sup>2</sup>.h flux with 71.23% rejection for 2000 ppm solution of boric acid and 80.68 L/m<sup>2</sup>.h flux with 98.96% rejection for 1000 ppm solution of humic acid at 1.5 MPa. The rejection of sulfate ions containing salts (MgSO<sub>4</sub>, Na<sub>2</sub>SO<sub>4</sub>, MnSO<sub>4</sub>, CuSO<sub>4</sub>) is much higher than chloride ion containing salt due to synergistic effect of strong Donnan exclusion and size sieving of sulfate ions. When we chose NaCl as a feed solution with 2000 ppm feed concentration, the high flux and low rejection observed. Because nanofiltration membrane separation performance for electrolyte solution ion is mostly strongminded by Donnan exclusion effect and steric hindrance [69,70]. It is also know that the Donnan effect and size exclusion plays a very important role in salt rejection of nanofiltration membranes. Moreover, in the case of charged NF membranes, the electrostatic repulsion also has an effect on the salt rejection. Therefore it is found that, the change of surface zeta potential of modified NF membranes would result in the variation of salts rejection. With different incorporation sites of nanomaterials, the dominant mechanism is different for the TFN membranes. Therefore, it is realistic conclude that Donnan equilibrium and dielectric repulsion are the key assistances to the salt

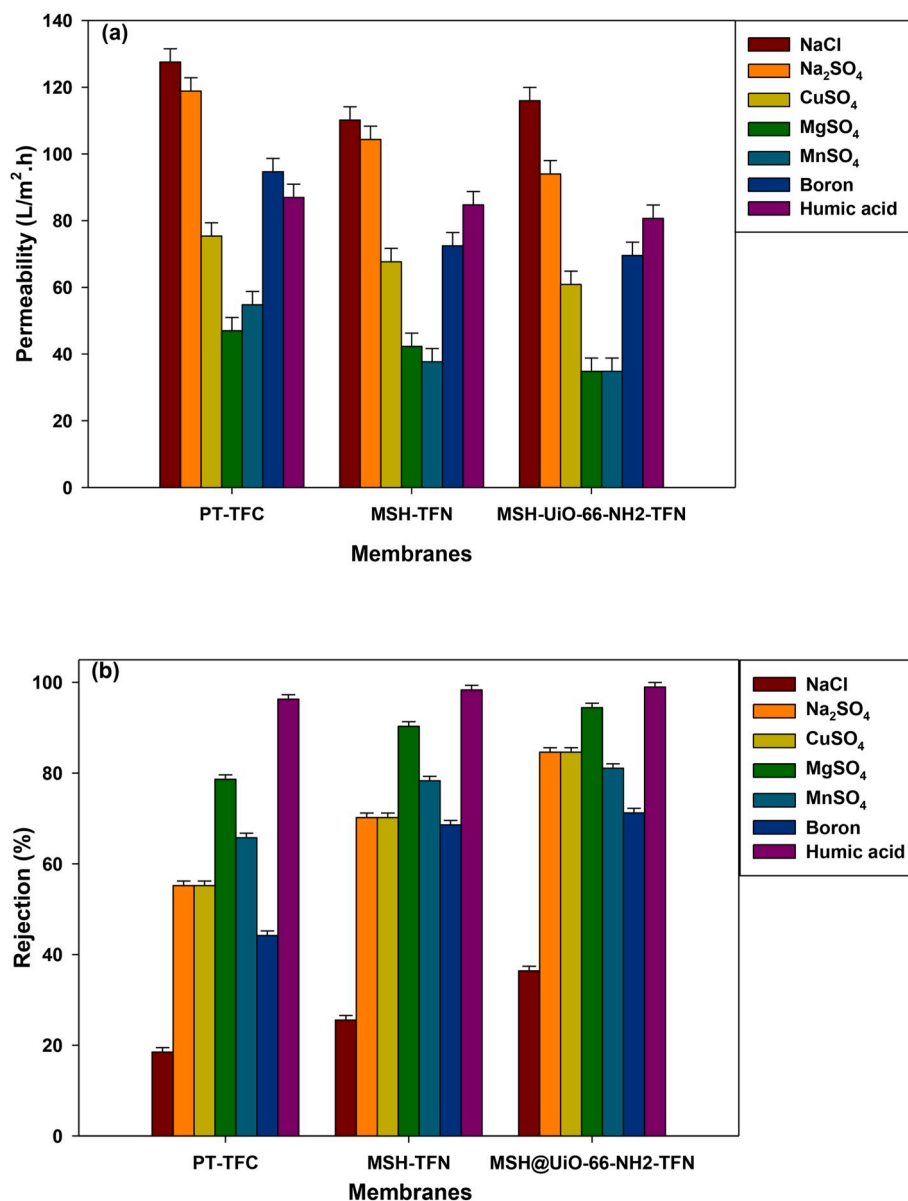


Fig. 10. (a) Permeation fluxes and (b) Rejection with different salt solution of the PT-TFC, MSH-TFN, and MSH@UiO-66-NH<sub>2</sub>-TFN membranes.

separation for all these tested membranes. The incorporation of MSH and MSH@UiO-66-NH<sub>2</sub> into the PA layer increase the flux and salt rejection and detected styles are dependable with the mechanism of Donnan equilibrium and dielectric repulsion. In difference, compare with PT-TFC the MSH-TFN and MSH@UiO-66-NH<sub>2</sub>-TFN membranes the permeate flux slightly reduce but the salt rejections are alluringly enhanced.

As explain in Donnan exclusion theory for the solution of single salt a higher valence co-ion (i.e. bivalent salt) causes high rejection and in high valence counter-ion leads a low rejection of salt (monovalent salt so obtained results are 115.9 L/m<sup>2</sup>.h flux and 36.4% NaCl rejection for MSH@UiO-66-NH<sub>2</sub>-TFN membrane) [71]. Here in TFN membrane case the negative selective layer applies an electrostatic repulsion on the anion. Therefore to maintain electrical neutrality for every repelled anion, it must be balanced by cation [72]. So as a results the prepared nanofiltration membranes continuously shows the high rejection for bivalent salt molecules as obtained in our present research work and low rejection of monovalent salts as shown in Fig. 10 (b).

On the basis of characterization result it is found that due to synergistic textural properties results of mixed nanoparticles on MSH@UiO-

66-NH<sub>2</sub>-TFN membrane is more hydrophilic and as expected the improved flux and rejection (flux is not drastically change compare with PT-TFC membrane). In details, MSH@UiO-66-NH<sub>2</sub>-TFN shows 98.96% rejection of humic acid with 80.86 L/m<sup>2</sup>.h water flux due to the increasing polymer cross-link density [73]. As known at pH 8 the most of the boron molecules were uncharged, hence we inferred that the absorbed boron by TFN layer will not pass through the membranes pores [22,74]. As already explained above removal of boron from water is challenging task even though our lab developed nanocomposite membranes showed excellent performance in the form of rejection and permeability against high concentrated boric acid feed solution. Especially the concentration is given for boron and humic acid rejection without compromising the water flux. The experiment conducted by consider of the MgSO<sub>4</sub> separation test and it is found that by using TFC membrane the obtained flux was about 47.0 L/m<sup>2</sup>.h with rejection rate about 78.63%. After addition of MSH nanoparticles the membrane performance was increase up to 42.3 L/m<sup>2</sup>.h flux and 90.32% rejection. The drastic change is observed while using MSH@UiO-66-NH<sub>2</sub>-TFN membrane case here the flux 34.78 L/m<sup>2</sup>.h and rejection 94.42% was obtain when tested with 2000 ppm solution at 1.5 MPa pressure at room



temperature.

### 3.5. Effect of operating pressure on water flux and rejection

The variations of water flux and salt rejection of the TFC and TFN membranes with the operation pressure were studied using  $\text{Na}_2\text{SO}_4$  and  $\text{MgSO}_4$  as feed solutions. The permeability variation of TFC and TFN

membranes were found as operating pressure varies from 0.5 to 2.0 MPa. It is found that the flux performances of membranes increased with operating pressure.

As shown in Fig. 11 (a) the result of 2000 ppm  $\text{Na}_2\text{SO}_4$  feed solution with different operating pressure, the highest fluxes were found at pressure 2.0 MPa i. e. 131.3  $\text{L}/\text{m}^2\cdot\text{h}$ , 123.4  $\text{L}/\text{m}^2\cdot\text{h}$ , and 111.3  $\text{L}/\text{m}^2\cdot\text{h}$  for PT-TFC, MSH-TFN and MSH@UiO-66- $\text{NH}_2$ -TFN membranes

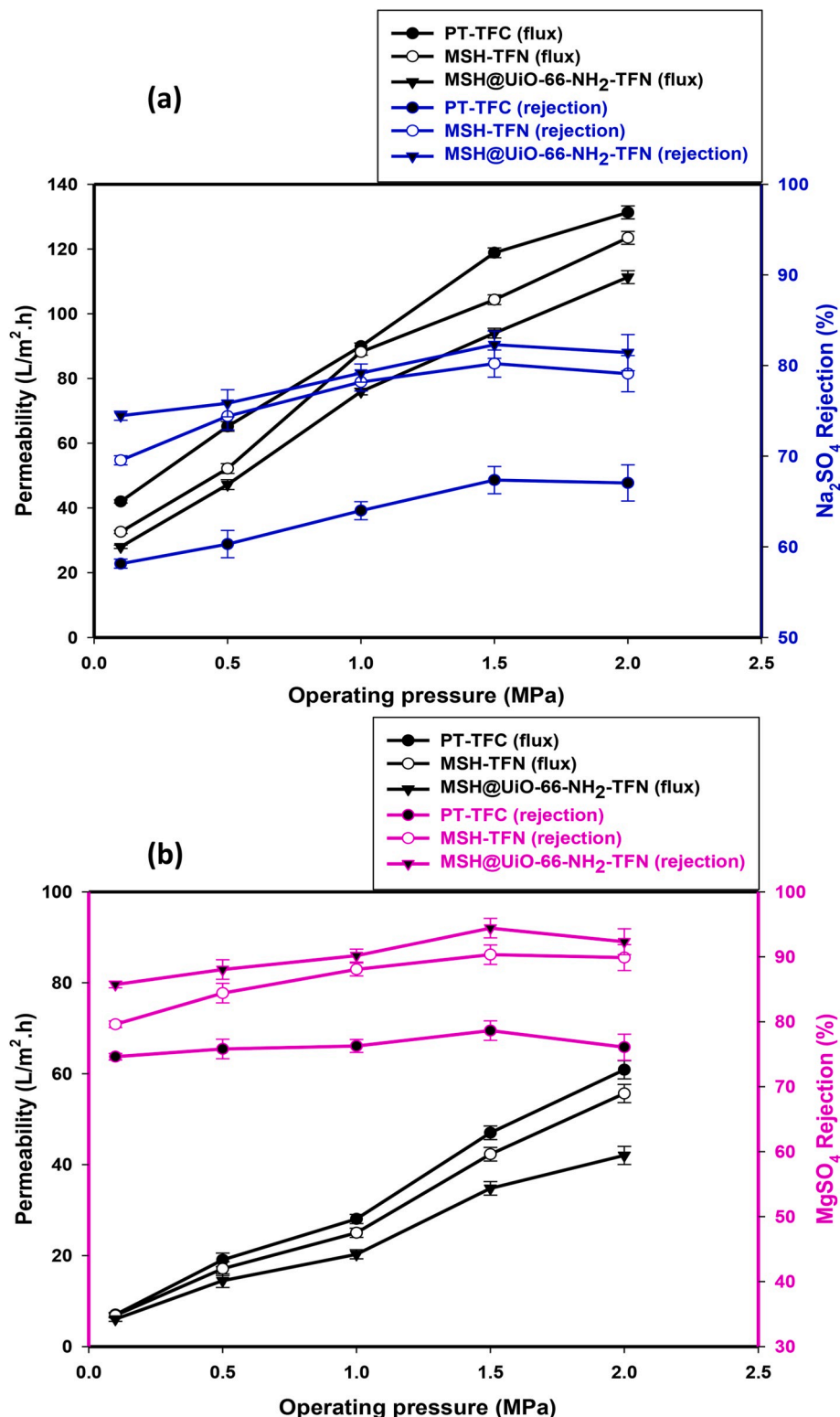


Fig. 11. Variations of water flux and salt rejection with (a)  $\text{Na}_2\text{SO}_4$  and (b)  $\text{MgSO}_4$  of the TFC and TFN membranes with the variable operation pressure.

respectively. The highest  $\text{Na}_2\text{SO}_4$  rejections were found at pressure 1.5 MPa i.e. 67.3%, 80.2% and 82.2% for PT-TFC, MSH-TFN and MSH@UiO-66-NH<sub>2</sub>-TFN membranes respectively. Same membrane was tested for  $\text{MgSO}_4$  feed solution after varying the operating pressure from 0.5 to 2.0 MPa having concentration 2000 ppm. The obtained results as shown in Fig. 11 (b), it is observed that the highest fluxes are obtained at pressure 2.0 MPa i.e. for PT-TFC 60.9 L/m<sup>2</sup>.h, MSH-TFN 55.7 L/m<sup>2</sup>.h and for MSH@UiO-66-NH<sub>2</sub>-TFN membrane 42.0 L/m<sup>2</sup>.h. The highest rejection was obtained at pressure 1.5 MPa i.e. 78.6%, 90.3% and 94.4% for PT-TFC, MSH-TFN and MSH@UiO-66-NH<sub>2</sub>-TFN membranes respectively. The obtained results shows the rejection was auxiliary enhanced at higher pressure up to 1.5 MPa after that slightly decreased at 2.0 MPa due to fast transport of salt molecules. The prepared interfacially polymerized membranes shows great potential to facing the challenge of making the TFN membranes as stable, robust, accessible, and cost-effective as their polymeric equivalents in the form of current RO membrane technologies [75].

### 3.6. Boron rejection by TFN membranes

Fig. 12 (a) shows the result of flux and 12 (b) shows the boron rejection using PT-TFC, MSH-TFN, and MSH@UiO-66-NH<sub>2</sub>-TFN membranes. As a result, using MSH@UiO-66-NH<sub>2</sub>-TFN membranes, the highest 71.23% boron rejection was obtained. Here the above prepared TFN membranes shows high boron rejection because the presence of narrow nanochannels in the selective polyamide nanocomposite layer [76]. Therefore, the water molecules rapidly transport through the membrane and boron molecules becomes rejected. Here acid base electrostatic interaction theory and Zeta potential differences were also played an important role. In TFN membranes incorporated nanoparticles have narrow channels also create resistance for boron in permeate solution and as a result the high rejection rate is observed. As found in zeta potential result the TFN membranes found more negatively charge surfaces and lower contact angle so this is also one of the reason for high water flux and high rejection especially using MSH@UiO-66-NH<sub>2</sub>-TFN membrane. Compare the rejection rate in between TFN and TFC the TFN shows significantly improved boron rejection. Because the absorbed boron in MSH@UiO-66-NH<sub>2</sub> TFN nanochannel shows pore narrowing effect might be responsible to reduce the passage for small molecules like boron. Our present findings are found comparable with the previous reports [23,77,78].

### 3.7. Humic acid rejection by TFN membranes

Since in the above conducted experiment we further explore the applicability of the developed membranes for humic acid rejection and anti-organic fouling property. The experiments were carried out using pressure 1.5 MPa with 1000 ppm humic acid feed solution. As shown in Fig. 13 (a) it is found that up to 10 h there is not much reduction found in the water flux, it means MSH@UiO-66-NH<sub>2</sub>-TFN membrane has good antifouling properties. The real condition of all membranes after experiments are shown in Fig. S3, and it can clearly see the antifouling nature of TFN membranes. The humic acid rejection result of PT-TFC, MSH-TFN, and MSH@UiO-66-NH<sub>2</sub>-TFN membranes performance are shown in Fig. 13 (b). The TFC membrane exhibit slightly higher water flux (86.95 L/m<sup>2</sup>.h) compare with MSH-TFN (84.73 L/m<sup>2</sup>.h) and MSH@UiO-66-NH<sub>2</sub>-TFN membrane i.e. 80.68 L/m<sup>2</sup>.h with rejection efficiency in the range 96.3–98.96%. The addition of functional UiO-66 nanoparticles imparts the negative charge density and improved hydrophilicity of membrane [79,80]. It is also found that due to hydrophilicity of TFN membrane the interaction between TFN membrane and humic acid lessened, therefore permeability not much reduced only small change observed but rejection rate increased considerable. The detail comparison with examples of MOFs incorporated TFN membranes on various substrates has been added as a Table S1 in supporting information file.

### 3.8. Antibacterial activity of TFN membrane

The antibacterial activity of developed TFN membrane has been checked with *E. coli* BI21 (*Escherichia coli*) and the results are shown in Fig. 14. It's important to mention here that in the present investigation for the first time we checked either this MSH@UiO-66-NH<sub>2</sub> incorporated membrane might show any antibacterial property or not. As clearly found in Fig. 14(b) after 3 h dramatically bacterial colony reduction was observed (compared in between Fig. 14(a) initial and Fig. 14(b) after 3 h). It is due to direct MSH@UiO-66-NH<sub>2</sub> incorporated membrane contact physically interrupts the cells of the bacteria and also encourages apoptotic mechanisms by oxidative stresses, additionally it possibly due to defects/oxygen vacancy, charge transfer, membrane destruction, etc. Finally, we reconfirmed that due to anomalous characteristics (surface charge, functionalities as well as structural and textural differences etc.) of MSH@UiO-66-NH<sub>2</sub> modified membrane showed excellent antibacterial performance.

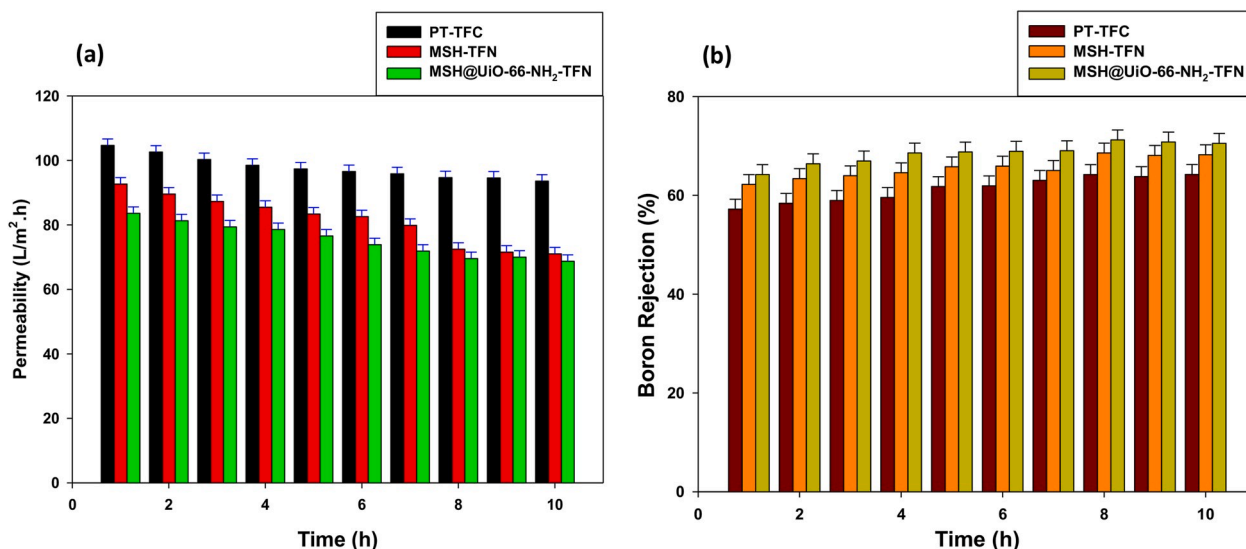


Fig. 12. (a) Permeability and (b) Rejection of boron against variable time at operating pressure 1.5 MPa.

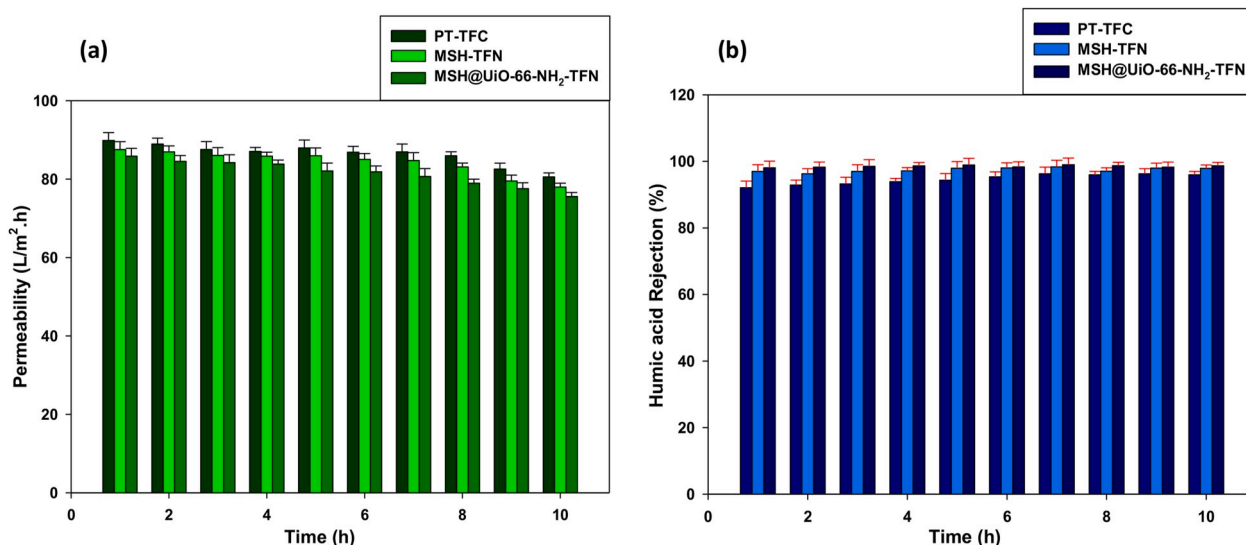


Fig. 13. (a) Permeability and (b) rejection of humic acid against variable time at operating pressure 1.5 MPa.

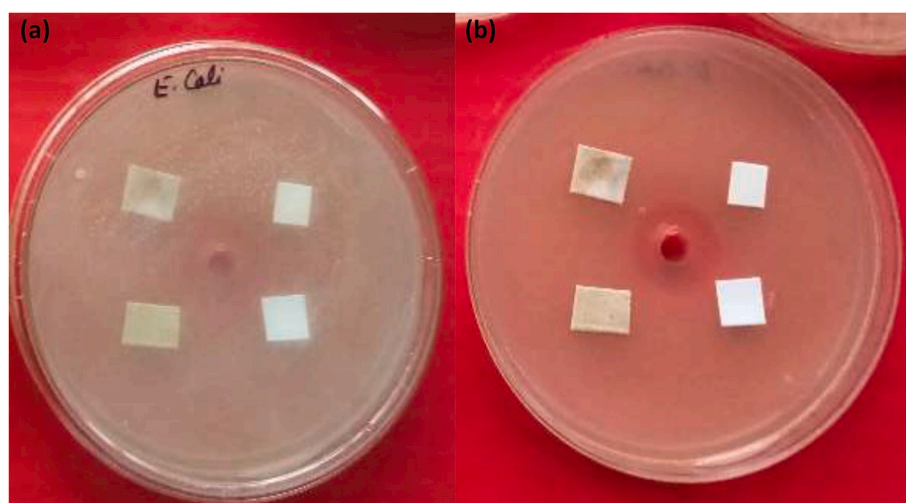


Fig. 14. Antibacterial property of the MSH@UiO-66-NH₂-TFN membrane estimated by the plate colony-forming count experiments (a) initial and (b) after 3 h.

#### 4. Conclusions

In this study the TFC and MSH, MSH@UiO-66-NH<sub>2</sub> incorporated TFN membranes successfully prepared, characterized and tested with different feed solutions. The separation experiments were done using various salt solutions (monovalent and bivalent), boron and humic acid. The antifouling and antibacterial study was also done and prepared membranes are found with both the properties with the enhanced results. Superior water fluxes and rejections were achieved by TFN membranes. The MSH@UiO-66-NH<sub>2</sub>-TFN membrane shown higher rejection than the MSH-TFN and TFC membrane. In this study it is also found that the MSH@UiO-66-NH<sub>2</sub> nanoparticles have substantial intrinsic narrow nanochannels and adsorption capacity for boron. In the case of humic acid also there are no sacrifices of water flux for long duration experiments. Therefore the conclusion is the prepared TFN membranes have good antifouling and antibacterial properties. The experimental finding also showed that after incorporating nanoparticles, the TFN membranes performance is not only good for boron rejection but also superlative for humic acid separation. The key finding of this study is the prepared TFN membranes have the noble capacity of high performance with various salts along with toxic boron, bulkier humic

acid separation and antibacterial properties.

#### Declaration of competing interest

The authors declare that they have no known competing financial interests or personal relationships that could have appeared to influence the work reported in this paper.

#### Acknowledgement

The authors are thankful to the Director, CSIR-NEIST, Jorhat for his continuous support and encouragement to carry out the work. Acknowledgement to Department of Science and Technology (DST), New Delhi, India under the Nano mission project DST/NM/NT/2018/143 (GPP-0357) and CSIR, India (CSIR-NEIST in-house project No. OLP 2021) for the financial support. The authors are also grateful for discussion and help to do antibacterial activity study of TFN membranes from Dr. S. B. Wann and Mrs. Archana Yadav (BSTD, CSIR-NEIST). Authors are also acknowledged the sophisticated analytical facilities of CSIR-NEIST, Jorhat, Assam, India.

## Appendix A. Supplementary data

Supplementary data to this article can be found online at <https://doi.org/10.1016/j.memsci.2020.118212>.

## References

- [1] J.A. Prince, S. Bhuvana, K.V.K. Boodhoo, V. Anbharasi, G. Singh, Synthesis and characterization of PEG-Ag immobilized PES hollow fiber ultrafiltration membranes with long lasting antifouling properties, *J. Membr. Sci.* 454 (2014) 538–548.
- [2] P.G. Ingole, Application of Sustainable Nanocomposites in Membrane Technology<sup>†</sup> Sustainable Polymer Composites and Nanocomposites, Springer Nature Switzerland (AG), 2019, ISBN 978-3-030-05399-4, pp. 935–960.
- [3] M.I. Baig, P.G. Ingole, J.D. Jeon, S.U. Hong, W.K. Choi, H.K. Lee, Water vapor transport properties of interfacially polymerized thin film nanocomposite membranes modified with graphene oxide and GO-TiO<sub>2</sub> nanofillers, *Chem. Eng. J.* 373 (2019) 1190–1202.
- [4] A. Inurria, P. Cay-Durgun, D. Rice, H. Zhang, D.K. Seo, M.L. Lind, F. Perreault, Polyamide thin-film nanocomposite membranes with graphene oxide nanosheets: balancing membrane performance and fouling propensity, *Desalination* 451 (2019) 139–147.
- [5] P.G. Ingole, M.I. Baig, W.K. Choi, X. An, W.K. Choi, H.K. Lee, Role of functional nanoparticles to enhance the polymeric membrane performance for mixture gas separation, *J. Ind. Eng. Chem.* 48 (2017) 5–15.
- [6] P.G. Ingole, H.C. Bajaj, K. Singh, Membrane separation processes: optical resolution of lysine and asparagine amino acids, *Desalination* 343 (2014) 75–81.
- [7] J. Zhu, L. Qin, A.A. Uliana, J. Hou, J. Wang, Y. Zhang, X. Li, S. Yuan, J. Li, M. Tian, Elevated performance of thin film nanocomposite membranes enabled by modified hydrophilic MOFs for nanofiltration, *ACS Appl. Mater. Interfaces* 9 (2017) 1975–1986.
- [8] F.Y. Zhao, Y.L. Ji, X.D. Weng, Y.F. Mi, C.C. Ye, Q.F. An, C.J. Gao, High-flux positively charged nanocomposite nanofiltration membranes filled with poly (dopamine) modified multiwall carbon nanotubes, *ACS Appl. Mater. Interfaces* 8 (2016) 6693–6700.
- [9] S.H. Park, Y.G. Park, J.L. Lim, S. Kim, Evaluation of ceramic membrane applications for water treatment plants with a life cycle cost analysis, *Des. Wat. Treat.* 54 (2015) 973–979.
- [10] S.H. Jamali, T.J.H. Vlucht, L.C. Lin, Atomistic understanding of zeolite nanosheets for water desalination, *J. Phys. Chem. C* 121 (2017) 11273–11280.
- [11] D. Qadir, H. Mukhtar, L.K. Keong, Mixed matrix membranes for water purification applications, *Separ. Purif. Rev.* 46 (2017) 62–80.
- [12] Z. Yang, X. Huang, X.H. Ma, Z.W. Zhou, H. Guo, Z. Yao, S.P. Feng, C.Y. Tang, Fabrication of a novel and green thin-film composite membrane containing nanovoids for water purification, *J. Membr. Sci.* 570–571 (2019) 314–321.
- [13] S. Abdikheibari, W. Lei, L.F. Dumée, N. Milne, K. Baskaran, Thin film nanocomposite nanofiltration membranes from amine functionalized-boron nitride/polypiperazine amide with enhanced flux and fouling resistance, *J. Mater. Chem.* 6 (2018) 12066–12081.
- [14] M.I. Baig, P.G. Ingole, J.D. Jeon, S.U. Hong, W. Choi, B. Jang, H.K. Lee, Water vapor selective thin film nanocomposite membranes prepared by functionalized Silicon nanoparticles, *Desalination* 451 (2019) 59–71.
- [15] O. Choi, P.G. Ingole, H.K. Lee, Preparation and characterization of thin film composite membrane for the removal of water vapor from the flue gas at bench scale, *Separ. Purif. Technol.* 211 (2019) 401–407.
- [16] A.M. Abou-Elanwar, Y.M. Shirke, P.G. Ingole, W.K. Choi, H. Lee, S.U. Hong, H. K. Lee, J.D. Jeon, Nanocomposite hollow fiber membranes with recyclable  $\beta$ -cyclodextrin encapsulated magnetite nanoparticles for water vapor separation, *J. Mater. Chem.* 6 (2018) 24569–24579.
- [17] L.D. Nghiem, P.J. Coleman, C. Ependiller, Mechanisms underlying the effects of membrane fouling on the nanofiltration of trace organic contaminants, *Desalination* 250 (2010) 682–687.
- [18] L.D. Nghiem, A.I. Schäfer, M. Elimelech, Role of electrostatic interactions in the retention of pharmaceutically active contaminants by a loose nanofiltration membrane, *J. Membr. Sci.* 286 (2006) 52–59.
- [19] Y. Cengelloglu, G. Arslan, A. Tor, I. Kocak, N. Dursun, Removal of boron from water by using reverse osmosis, *Separ. Purif. Technol.* 64 (2008) 141–146.
- [20] K.L. Tu, L.D. Nghiem, A.R. Chivas, Coupling effects of feed solution pH and ionic strength on the rejection of boron by NF/RO membranes, *Chem. Eng. J.* 168 (2011) 700–706.
- [21] N. Kabay, M. Bryjak, N. Hilal, Boron Separation Processes, first ed., Elsevier, 2015.
- [22] J.H. Hu, Y.L. Pu, M. Ueda, X. Zhang, L.J. Wang, Charge-aggregate induced (CAI) reverse osmosis membrane for seawater desalination and boron removal, *J. Membr. Sci.* 520 (2016) 1–7.
- [23] H. Hyung, J.H. Kim, A mechanistic study on boron rejection by sea water reverse osmosis membranes, *J. Membr. Sci.* 286 (2006) 269–278.
- [24] L.D. Nghiem, D. Vogel, S. Khan, Characterising humic acid fouling of nanofiltration membranes using bisphenol A as a molecular indicator, *Water Res.* 42 (2008) 4049–4058.
- [25] K.A. Gebru, C. Das, Removal of bovine serum albumin from wastewater using fouling resistant ultrafiltration membranes based on the blends of cellulose acetate, and PVP- TiO<sub>2</sub> nanoparticles, *J. Environ. Manag.* 200 (2017) 283–294.
- [26] C. Wang, Z. Li, J. Chen, Y. Yin, H. Wu, Structurally stable graphene oxide-based nanofiltration membranes with bioadhesive polydopamine coating, *Appl. Surf. Sci.* 427 (2018) 1092–1098.
- [27] W. Wang, L. Zhu, B. Shan, C. Xie, C. Liu, F. Cui, G. Li, Preparation and characterization of SLS-CNT/PES ultrafiltration membrane with antifouling and antibacterial properties, *J. Membr. Sci.* 548 (2018) 459–469.
- [28] Y. Wang, Q. Yang, J. Dong, H. Huang, Competitive adsorption of PPCP and humic substances by carbon nanotube membranes: effects of coagulation and PPCP properties, *Sci. Total Environ.* 619–620 (2018) 352–359.
- [29] L.C. Nuan, Q. Zhao, J. Liu, Y. Zhang, Antibacterial behavior of halloysite nanotubes decorated with copper nanoparticles in a novel mixed matrix membrane for water purification, *Environ. Sci.: Water Res. Technol.* 1 (2015) 874–881.
- [30] W.J. Lau, S. Gray, T. Matsuura, D. Emadzadeh, J.P. Chen, A.F. Ismail, A review on polyamide thin film nanocomposite (TFN) membranes: history, applications, challenges and approaches, *Water Res.* 80 (2015) 306–324.
- [31] C. Liu, J. Lee, J. Ma, M. Elimelech, Antifouling thin-film composite membranes by controlled architecture of zwitterionic polymer brush layer, *Environ. Sci. Technol.* 514 (2017) 2161–2169.
- [32] Z.C. Ng, C.Y. Chong, W.J. Lau, M. Karaman, A.F. Ismail, Boron removal and antifouling properties of thin-film nanocomposite membrane incorporating PECVD-modified titanate nanotubes, *J. Chem. Technol. Biotechnol.* 94 (2019) 2772–2782.
- [33] A. Shakeri, H. Salehi, F. Ghorbani, M. Amini, H. Nashedjani, Polyoxometalate based thin film nanocomposite forward osmosis membrane: superhydrophilic, anti-fouling, and high water permeable, *J. Colloid Interface Sci.* 536 (2019) 328–338.
- [34] Y.-F. Mi, Q. Zhao, Y.-L. Ji, Q.-F. An, C.-J. Gao, A novel route for surface zwitterionic functionalization of polyamide nanofiltration membranes with improved performance, *J. Membr. Sci.* 490 (2015) 311–320.
- [35] D. Li, J. Wu, S. Yang, W. Zhang, F. Ran, Hydrophilicity and anti-fouling modification of polyethersulfone membrane by grafting copolymer chains via surface initiated electrochemically mediated atom transfer radical polymerization, *New J. Chem.* 41 (2017) 9918–9930.
- [36] H. Ju, B.D. McCloskey, A.C. Sagle, Y.H. Wu, V.A. Kusuma, B.D. Freeman, Crosslinked poly(ethylene oxide) fouling resistant coating materials for oil/water separation, *J. Membr. Sci.* 307 (2008) 260–267.
- [37] M.N. Goushki, S.A. Mousavi, M.J. Abdekhoodae, M. Sadeghi, Free radical graft polymerization of 2-hydroxyethyl methacrylate and acrylic acid on the polysulfone membrane surface through circulation of reaction media to improve its performance and hemocompatibility properties, *J. Membr. Sci.* 564 (2018) 762–772.
- [38] M.L. Lind, D. Eumine Suk, T.V. Nguyen, E.M. Hoek, Tailoring the structure of thin film nanocomposite membranes to achieve seawater RO membrane performance, *Environ. Sci. Technol.* 44 (2010) 8230–8235.
- [39] A. Nguyen, L. Zou, C. Priest, Evaluating the antifouling effects of silver nanoparticles regenerated by TiO<sub>2</sub> on forward osmosis membrane, *J. Membr. Sci.* 454 (2014) 264–271.
- [40] H. Huang, X. Qu, H. Dong, L. Zhang, H. Chen, Role of NaA zeolites in the interfacial polymerization process towards a polyamide nanocomposite reverse osmosis membrane, *RSC Adv.* 3 (2013) 8203–8207.
- [41] S.G. Kim, D.H. Hyeon, J.H. Chun, B.H. Chun, S.H. Kim, Nanocomposite poly (arylene ether sulfone) reverse osmosis membrane containing functional zeolite nanoparticles for seawater desalination, *J. Membr. Sci.* 443 (2013) 10–18.
- [42] S.R. Lakhota, M. Mukhopadhyay, P. Kumari, Cerium oxide nanoparticles embedded thin-film nanocomposite nanofiltration membrane for water treatment, *Sci. Rep.* 8 (2018) 4976.
- [43] X. Liu, Metal-organic framework UiO-66 membranes, *Front. Chem. Sci. Eng.* 14 (2020) 216–232.
- [44] P.G. Ingole, M. Sohail, A.M. Abou-Elanwar, M.I. Baig, J.D. Jeon, W.K. Choi, H. Kim, H.K. Lee, Water vapor separation from flue gas using MOF incorporated thin film nanocomposite hollow fiber membranes, *Chem. Eng. J.* 334 (2018) 2450–2458.
- [45] R.R. Pawar, B.D. Kevadiya, H. Brahmabhatt, H.C. Bajaj, Template free synthesis of mesoporous hectorites: efficient host for pH responsive drug delivery, *Int. J. Pharmacol.* 446 (2013) 145–152.
- [46] R.R. Pawar, H.A. Patel, G. Sethia, H.C. Bajaj, Selective adsorption of carbon dioxide over nitrogen on calcined synthetic hectorites with tailor-made porosity, *Appl. Clay Sci.* 46 (2009) 109–113.
- [47] G.V. Joshi, R.R. Pawar, B.D. Kevadiya, H.C. Bajaj, Mesoporous synthetic hectorites: a versatile layered host with drug delivery application, *Microporous Mesoporous Mater.* 142 (2011) 542–548.
- [48] S.Y. Sawant, R.R. Pawar, R.S. Somani, H.C. Bajaj, Facile hard template approach for synthetic hectorite hollow microspheres, *Mater. Lett.* 128 (2014) 121–124.
- [49] R.R. Pawar, P. Gupta Lalhmunsiani, S.Y. Sawant, B. Shahmoradi, S.M. Lee, Porous synthetic hectorite clay-alginate composite beads for effective adsorption of methylene blue dye from aqueous solution, *Int. J. Biol. Macromol.* 114 (2018) 1315–1324.
- [50] K.A. Carrado, Synthetic organo- and polymer-clays: preparation, characterization, and materials applications, *Appl. Clay Sci.* 17 (2000) 1–23.
- [51] I. Vicente, P. Salagre, Y. Cesteros, F. Guirado, F. Medina, J. Sueiras, Fast microwave synthesis of hectorite, *Appl. Clay Sci.* 43 (2009) 103–107.
- [52] M. Thommes, K. Kaneko, V. Neimark Alexander, P. Olivier James, F. Rodriguez-Reinos, J. Rouquerol, S.W. Sing Kenneth, Physiosorption of gases, with special reference to the evaluation of surface area and pore size distribution (IUPAC Technical Report), *Pure Appl. Chem.* 87 (2015) 1051–1069.
- [53] M. Kim, J.F. Cahill, K.A. Prather, S.M. Cohen, Postsynthetic modification at orthogonal reactive sites on mixed, bifunctional metal-organic frameworks, *Chem. Com.* 47 (2011) 7629–7631.



- [54] M.A. Bunge, A.B. Davis, K.N. West, C.W. West, T.G. Glover, Synthesis and characterization of UiO-66-NH<sub>2</sub> metal-organic framework cotton composite textiles, *Ind. Eng. Chem. Res.* 57 (2018) 9151–9161.
- [55] D.C. Ma, S.B. Peh, G. Han, S.B. Chen, Thin-Film nanocomposite (TFN) membranes incorporated with super-hydrophilic metal-organic framework (MOF) UiO-66: toward enhancement of water flux and salt rejection, *ACS Appl. Mater. Interfaces* 9 (2017) 7523–7534.
- [56] D.X. Trinh, T.P.N. Tran, T. Taniike, Fabrication of new composite membrane filled with UiO-66 nanoparticles and its application to nanofiltration, *Separ. Purif. Technol.* 177 (2017) 249–256.
- [57] S.J. Garibay, S.M. Cohen, Isoreticular synthesis and modification of frameworks with the UiO-66 topology, *Chem. Com.* 46 (2010) 7700–7702.
- [58] K.Y.A. Lin, Y.T. Liu, S.Y. Chen, Adsorption of fluoride to UiO-66-NH<sub>2</sub> in water: stability, kinetic, isotherm and thermodynamic studies, *J. Colloid Interface Sci.* 461 (2016) 79–87.
- [59] A.S. Bhatt, P.L. Sakaria, M. Vasudevan, R.R. Pawar, N. Sudheesh, H.C. Bajaj, H. M. Mody, Adsorption of an anionic dye from aqueous medium by organoclays: equilibrium modeling, kinetic and thermodynamic exploration, *RSC Adv.* 2 (2012) 8663–8671.
- [60] P.G. Ingole, H.C. Bajaj, D.N. Srivastava, B. Rebary, K. Singh, Preparation of thin film polymer composite membranes for optical resolution of racemic mixture of  $\alpha$ -amino acids, *Separ. Sci. Technol.* 48 (2013) 1777–1787.
- [61] D.C. Ma, S.B. Peh, G. Han, S.B. Chen, Thin-Film nanocomposite (TFN) membranes incorporated with super-hydrophilic metal-organic framework (MOF) UiO-66: toward enhancement of water flux and salt rejection, *ACS Appl. Mater. Interfaces* 9 (2017) 7523–7534.
- [62] C.Y. Tang, Y.N. Kwon, J.O. Leckie, Probing the nano- and micro-scales of reverse osmosis membranes-A comprehensive characterization of physiochemical properties of uncoated and coated membranes by XPS, TEM, ATR-FTIR, and streaming potential measurements, *J. Membr. Sci.* 287 (2007) 146–156.
- [63] K. Bousou, A. Brlpaire, A. Volodin, C.V. Haesendonck, P. van der Meeren, C. Vandecasteele, B. van der Bruggen, Influence of membrane and colloid characteristics on fouling of nanofiltration membranes, *J. Membr. Sci.* 289 (2007) 220–230.
- [64] L. Yan, Y.S. Li, C.B. Xiang, S. Xianda, Effect of nano-sized Al<sub>2</sub>O<sub>3</sub>-particle addition on PVDF ultrafiltration membrane performance, *J. Membr. Sci.* 276 (2006) 162–167.
- [65] P.G. Ingole, R.R. Pawar, M.I. Baig, J.D. Jeon, B. Jang, H.K. Lee, Thin film nanocomposite (TFN) hollow fiber membranes incorporated with functionalized acid-activated bentonite (ABn-NH) clay: towards enhancement of water vapor permeance and selectivity, *J. Mater. Chem.* 5 (2017) 20947–20958.
- [66] K.P. Wai, C.H. Koo, Y.L. Pang, W.C. Chong, W.J. Lau, Synthesizing Ag/PDA/PES antibacterial membrane for natural organic molecules removal, in: *E3S Web Conf.*, vol. 65, 2018, 05023.
- [67] J. Yin, E.-S. Kim, J. Yang, B. Deng, Fabrication of a novel thin-film nanocomposite (TFN) membrane containing MCM-41 silica nanoparticles (NPs) for water purification, *J. Membr. Sci.* 423–424 (2012) 238–246.
- [68] D. Li, H.Y. Zhu, K.R. Ratnac, S.P. Ringer, H. Wang, Synthesis and characterization of sodalite-polyimide nanocomposite membranes, *Microporous Mesoporous Mater.* 126 (2009) 14–19.
- [69] R. Xu, P. Zhang, Q. Wang, X.M. Wang, K.C. Yu, T. Xue, X.H. Wen, Influences of multi influent matrices on the retention of PPCPs by nanofiltration membranes, *Separ. Purif. Technol.* 212 (2019) 299–306.
- [70] V.S. Kumar, K.S. Hariharan, K.S. Mayya, S.S. Han, Volume averaged reduced order Donnan Steric Pore Model for nanofiltration membranes, *Desalination* 322 (2013) 21–28.
- [71] D.X. Wang, M. Su, Z.Y. Yu, X.L. Wang, M. Ando, T. Shintani, Separation performance of a nanofiltration membrane influenced by species and concentration of ions, *Desalination* 175 (2005) 219–225.
- [72] Z.K. Yao, H. Guo, Z. Yang, W.H. Qing, C.Y. Tang, Preparation of nanocavity-contained thin film composite nanofiltration membranes with enhanced permeability and divalent to monovalent ion selectivity, *Desalination* 445 (2018) 115–122.
- [73] M.I. Baig, P.G. Ingole, W.K. Choi, J.D. Jeon, B. Jang, J.H. Moon, H.K. Lee, Synthesis and characterization of thin film nanocomposite membranes incorporated with surface functionalized silicon nanoparticles for improved water vapor permeation performance, *Chem. Eng. J.* 308 (2017) 27–39.
- [74] R. Bernstein, S. Belfer, V. Freger, Toward improved boron removal in RO by membrane modification: feasibility and challenges, *Environ. Sci. Technol.* 45 (2011) 3613–3620.
- [75] Y. Lin, Y. Chen, R. Wang, Thin film nanocomposite hollow fiber membranes incorporated with surface functionalized HKUST-1 for highly-efficient reverse osmosis desalination process, *J. Membr. Sci.* 589 (2019) 117249.
- [76] G.S. Lai, W.J. Lau, S.R. Gray, T. Matsuura, R. Jamshidi Gohari, M.N. Subramanian, S.O. Lai, C.S. Ong, A.F. Ismail, D. Emazadah, M. Ghanbari, A practical approach to synthesize polyamide thin film nanocomposite (TFN) membranes with improved separation properties for water/wastewater treatment, *J. Mater. Chem.* 4 (2016) 4134–4144.
- [77] Z.C. Ng, C.Y. Chong, W.J. Lau, M. Karaman, A.F. Ismail, Boron removal and antifouling properties of thin-film nanocomposite membrane incorporating PECVD-modified titanate nanotubes, *J. Chem. Technol. Biotechnol.* 94 (2019) 2772–2782.
- [78] L. Liu, X. Xie, S. Qi, R. Li, X. Zhang, X. Song, C. Gao, Thin film nanocomposite reverse osmosis membrane incorporated with UiO-66 nanoparticles for enhanced boron removal, *J. Membr. Sci.* 580 (2019) 101–109.
- [79] J. Shao, J. Hou, H. Song, Comparison of humic acid rejection and flux decline during filtration with negatively charged and uncharged ultrafiltration membranes, *Water Res.* 45 (2011) 473–482.
- [80] C. Zhao, C.Y. Tang, P. Li, P. Adrian, G. Hu, Perfluorooctane sulfonate removal by nanofiltration membrane-the effect and interaction of magnesium ion/humic acid, *J. Membr. Sci.* 503 (2016) 31–41.